A Study of SAM Modified ZnO in Hybrid Bilayer ZnO/P3HT Photovoltaic Devices

by

Yousef Alattar

Submitted in partial fulfilment of the requirements
for the degree of Master of Applied Science

at

Dalhousie University
Halifax, Nova Scotia
July 2013

"Inspire me, O gods, and spin me a thread from the world's beginning" - Ovid

This thesis is dedicated to my family and friends, without them I would not have made it this far.

TABLE OF CONTENTS

LIST OF TABLES

LIST OF FIGURES

ABSTRACT

Hybrid organic/inorganic solar cells such as ZnO/P3HT offer promise in increasing efficiency of organic-based devices. However there are many unresolved issues such as poor short-circuit current and open-circuit voltage that are hampering their widespread, commercial use. It is thought that surface trap states on ZnO are providing an open avenue for carrier recombination thus creating devices with poor current transport characteristics. Using self assembled monolayers (SAMs) may provide some key answers and solutions to this problem by passivating trap states. In the course of this work, benzoic acid, 4-aminobenzoic acid, 4-methoxybenzoic acid, phenylphosphonic acid, and 4-methoxyphenylphosphonic acid SAMs were studied in large part due to their commercial availability. It was found that the phenylphosphonic acids had a clear impact on decreasing dark current; therefore strongly suggesting that exciton recombination has been inhibited to some degree. These molecules also caused a decrease in efficiency by an order of magnitude as compared to a plain ZnO/P3HT bilayer cell (standard). There were pronounced negative effects on the other device parameters such as open circuit voltage and short circuit current. In the case of 4-methoxybenzoic acid and benzoic acid the effects are not so clear in that parts of the dark J-V curve indicate a decrease in dark current while other regions show an increase. Interestingly for the negative effect on efficiency and other device parameters was not as pronounced as the phenylphosphonic acids. In both cases it is hypothesized that because of their wide band gaps and poor energy level matching, they ultimately impact device performance negatively. In the future, use of simulations to determine optimal SAM molecular structures that can be synthesized in the lab or purchased commercially is suggested.

LIST OF ABBREVIATIONS USED

IEA	International Energy Agency
OPV	Organic Photovoltaic
ZnO	Zinc Oxide
OLED	Organic Light Emitting Diode
OS	Organic Semiconductors
P3HT	Poly(3-hexylthiophene-2,5-diyl)
HOMO	Highest Occupied Molecular Orbital
LUMO	Lowest Unoccupied Molecular Orbital
UPS	Ultraviolet Spectroscopy
IPES	Inverse Photoelectron Spectroscopy
KE	Kinetic Energy
ITO	Indium doped Tin Oxide
V_{oc}	Open circuit voltage
J_{sc}	Short circuit current
FF	Fill Factor
η	Efficiency
SAM	Self Assembled Monolayer
RIE	Reactive Ion Etcher
RF	Radio Frequency
MEA	Monoethanolamine
STM	Sycon Thickness Monitor

ACKNOWLEDGEMENTS

I would like to thank my supervisor and co-supervisor, Dr. Ian Hill and Dr. Peter Gregson, for their support and advice throughout my project. I would like to thank Dr. Jeff Dahn for allowing me the use of his equipment. I would also like to thank all group members, especially Hafeez Anwer for keeping me grounded during some of the more difficult times over the course of this project.

CHAPTER 1 INTRODUCTION

Solar cells are needed in a future that is to be dominated by sustainable energy. The unstable nature of the fossil fuel economy and the effects of global warming are driving research in the area. The International Energy Agency (IEA) projects that by 2050 10% of global electricity will be supplied by solar-based technologies.[1] For this to become a reality, rapid progress in materials research is necessary to make solar technology affordable and readily available to the public.

At the present the solar cell industry is dominated by inorganic-based materials such as doped Si and CdTe. Hindering its more widespread use are the monetary and environmental cost of fabrication and the scarcity of materials needed to make these cells. Inorganics require an ultraclean environment, high temperatures, and batch process fabrication. Organic (or polymer-based) photovoltaics (OPVs) seem to be the natural solution to these issues.

OPVs may provide the solution because polymers are relatively simple and potentially cheap to fabricate and process in a large-scale industrial setting. With polymer-based materials, it is possible to have roll-to-roll fabrication processes and therefore have a continuous assembly line of OPVs.[2] It is a new technology (1986)[3] and there are several major hurdles to overcome before OPVs become commercially viable, such as low efficiencies and fast degradation times. It is important to note that OPVs are still in their technological infancy and great strides have been made in efficiency over the past two decades, with up to 10% efficiency being reported in the literature.[4] This is quite significant when one considers that the first organic solar cells were several orders of magnitude less efficient.

There are several different types of cell structures that are utilized in the literature. In the course of this work, hybrid inorganic/organic, ZnO/P3HT, bilayer solar cells were fabricated and characterized. The bilayer structure was used because of the ease of analysis of such a simple design. The hybrid inorganic/organic materials were used in this

work because combined they have the potential to offer a solar cell with the flexibility of organics with the advantage of being able to physically and chemically modify the more robust inorganic material. In addition inorganics have higher electron mobilities than their organic counterparts and this fact could drive organic solar cells to become more efficient. In particular ZnO was used because it is cheap, easy to make, and can be deposited from solution.[5]

It should be noted that organic electronics are starting to dominate what once were traditionally inorganic material domains. A notable case is the organic light emitting diodes (OLEDs). OLEDs are now incorporated into colour cell phones, dive computers, and even in fashion designs to name a few applications. If OLEDs provide an indication of the future of OPVs then it will truly be bright.

This dissertation is divided into five chapters. The second chapter delves into the theory of bilayer organic-inorganic OPVs and the effects of SAM modification at the organic-inorganic interface. The third chapter discusses the materials and methods involved in device fabrication and analysis. The fourth chapter is a presentation and discussion of the data collected. Lastly, the fifth chapter provides a conclusion and future research avenues that this project could take.

CHAPTER 2 ORGANIC PHOTOVOLTAIC THEORY

Solar cells, whether they are organic or inorganic, function using the same fundamental set of physical principles. Light must enter and be absorbed by the device. Secondly, the absorbed light will excite an electron in the active material. The excited electron will then be collected at a cathode, traverse an external circuit, and then travel to the anode. There is energy transfer in the materials that occurs before the excited electron reaches the cathode, a measured open circuit voltage results from this process. If too much energy is given away because of poor band matching characteristics between materials a poor open circuit voltage will result. The opposite needs to be true for good open circuit voltage values. A current is produced by the electron itself. When the electron is excited it leaves a hole in the once filled valence level. Holes are collected by the anode. Device efficiency is determined by the device's ability to absorb light effectively, harness charge at the electrodes, and the level of energy transfer in the materials (determining factor for open circuit voltage) before the electron goes to the cathode.[6,7]

2.1 Semiconductor Processes in Organics

2.1.1 Absorption and Molecular Structure

Organic semiconductors (OS) have relatively high absorption coefficients on the order of 10^5 cm^{-1} or greater. This property allows for device structures that have less than 100 nm of OS material while still being able to absorb most of the incident light. The chemical flexibility of OS allows for many possibilities for researchers in terms of choosing or fabricating a material for a particular absorption region.

The reason OS have such high absorption coefficients is because of their planar, aromatic (alternating single and double bond) structure. In Figure 1 Poly(3-hexylthiophene-2,5-diyl) (P3HT), the organic polymer used in the course of this work, is shown in Figure 1.

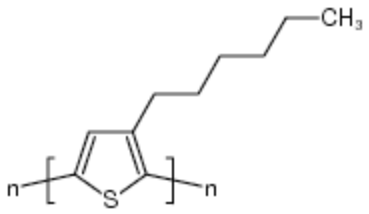

Figure 1: P3HT[8]

In these types of materials the sp^2-hybridization of carbon atoms and the resulting π-manifolds formed by p_z orbitals is the reason for abilities of these materials to absorb light in the ultraviolet (UV)-visible section of the solar spectrum and to transport current. Conduction along the molecule is a result of the bonding π orbitals, known as the highest occupied molecular orbital (HOMO), and the antibonding π*, known as the lowest unoccupied molecular orbital (LUMO). The π orbital electrons are free to move between atoms, strengthening the bonds. Delocalized orbitals are generated because there are states of equal potential between alternating single and double bonds. Charge transport in the molecule occurs because of these HOMO and LUMO levels. Once a photon is absorbed by these types of structures an electrostatically bound electron-hole pair, termed an exciton, is produced. [6,7]

2.1.2 Excitation

The delocalized nature of orbitals in each molecule and the relative lack of overlap between molecules means that an excited electron and hole are typically limited to a single molecule. The electrostatically bound electron-hole pair, attracted to each other due to Coulombic forces, is bound in a molecule and termed a Frenkel exciton. The binding energy of this quasi particle is 0.1 to 1 eV and is much larger than the thermal background energy, k_BT, of $1/40^{th}$ of an eV. Where k_B is Boltzmann's constant and T is temperature in Kelvin. As a result of this binding energy there is a difference between the optical band gap and charge transport gap. The charge transport gap takes into account the optical band gap and the exciton binding energy. This is the total energy needed to

generate free charge carriers. All band diagrams shown in the remainder of this thesis are optical band gaps as it is an accepted convention. Energy, besides the initial photon energy to generate the exciton, is needed to break the Coulomb attraction between the electron-hole pair.[2,5,6,7]

Organic materials' HOMO and LUMO levels can be measured using techniques such as ultraviolet photoelectron spectroscopy (UPS) and inverse photoemission spectroscopy (IPES). In UPS to determine the LUMO level the optical band gap is added to the measured HOMO level. Alternatively IPES can be used to measure the HOMO level directly. Briefly, UPS works by utilizing photons of known wavelength to photoexcite electrons from an atom or molecule. The emitted electron has a kinetic energy dependent on the original binding energy of the electron in the solid. This energy of outgoing electron of an outgoing electron is measured via a hemispherical analyser. The way it works is that different voltages are supplied to two hemispheres, one concave and the other convex with their centers of curvature coincident, creating an electric field between them. Slow electrons go to the inner sphere and faster electrons to the outer one, leaving only a narrow range of electrons (of an energy termed the pass energy) that are able to reach the detector.[9] . The energy from the photons is known ($h\upsilon$), the kinetic energy (KE) of outgoing electrons from the solid is measured, and binding energy is calculated by subtracting KE from $h\upsilon$. This is the binding energy of the HOMO.[2,6,7]

2.2.3 Diffusion

An applied electric field will not affect an exciton because of its overall charge neutrality and high binding energy. To disassociate an exciton a field on the order of 10^6 V/cm is required and neutrality counteracts any sort of drift phenomenon that would be experienced by either electron or hole. Excitons move through a random diffusive process jumping from one molecule to another. It is a relatively slow process and is one of the hindering aspects of OPVs. There is also a limited lifetime and therefore a limited length of travel that these quasi particles have before they recombine. The diffusion

length for most organics is below 20 nm; for P3HT it is approximately 10 nm. Recombination energy is emitted in the form of a photon or thermal energy to the molecule and surrounding molecular structure. Diffusive processes are what allow excitons to get to an energetically favourable area to break the Coulombic forces keeping it together; this will be explained further in the following sections.[2,6,7]

2.2.4 Dissociation

In OPVs excitons dissociate (the breaking of the Coulombic forces between an electron-hole pair) most effectually at the interface of two different materials when the energies are favoured. The electron affinity (EA) and ionization potential (IP) from the LUMO and HOMO levels respectively must differ between materials. This variation causes a band offset at the interface and if that offset is larger than the exciton binding energy dissociation will occur. The Coulombic attraction between electron and hole will be overcome, they will jump from one material's molecule to the other, and free charge carriers are generated. The labels of donor and acceptor are given based on the band offset of the given materials. An acceptor material gains an electron or loses a hole, and a donor materials donates an electron or gains a hole during the dissociation process. An organic material is not intrinsically a donor or acceptor; this is only determined when it is paired with another material. In particular it is the difference in electron affinities that determines its type. This is more clearly illustrated in Figure 2.[3,6,7]

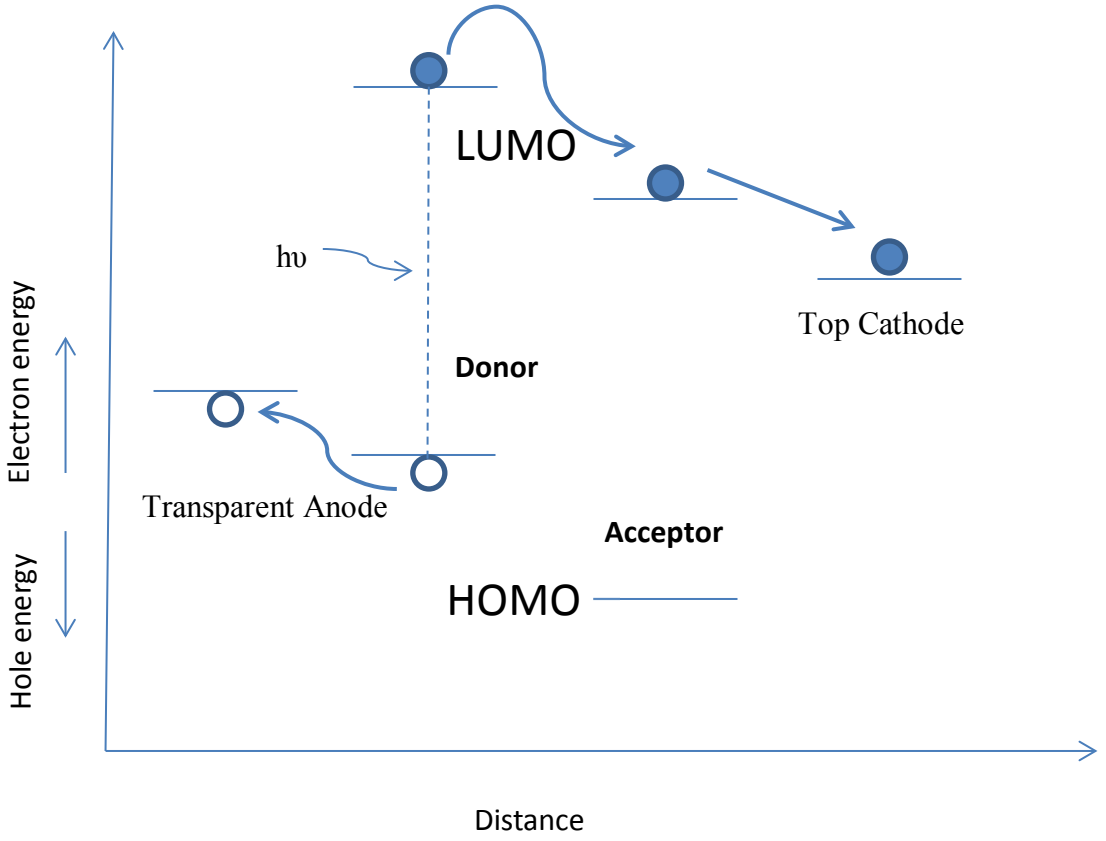

Figure 2: Dissociation occurring at the donor-acceptor interface. An exciton is generated in the donor material and the electron moves through the LUMO level while hole moves through the HOMO level. Electrons are represented by filled circles and holes by empty ones. Arrows are pointing in direction of increasing energy

2.2.5 Charge Collection and Transport

After exciton dissociation, free charge carriers are collected at the electrodes. A difference in work functions of the contacts causes an internal electric field. As a result the charge carriers drift toward their respective metal contacts. Higher charge collection efficiencies are achieved through large work function differences which correlate to greater electric fields. It is important to note that in order for an exciton to be generated a photon must reach the active organic material. As such one contact must be transparent in order to allow photons to reach the material.[2,7]

2.2 Key Solar Cell Parameters

Organic photovoltaics face many issues especially concerning the dissociation of excitons, collection of the free charge carriers after separation, and energy level compatibility between donor and acceptor (which determines open circuit voltage). These factors limit OPV performance. The power output is determined by these processes because power is dependent on current and voltage (P = IV). The OPV research community has gone to great lengths to improve output voltage and current characteristics of devices. The key parameters that will be discussed in the following sections are open circuit voltage (V_{OC}), short circuit current (J_{SC}), fill factor (FF), and efficiency (η).

2.2.1 Open Circuit Voltage

Open circuit voltage is defined in devices when there is no current flowing through the external circuit while a solar cell is being illuminated. The V_{OC} is dependent on the offset between the LUMO of the acceptor and the HOMO of the donor and has a partial dependence on the electrode work functions. The maximum energy that can be harvested depends on the energy difference in the acceptor's LUMO and the donor's HOMO.[6, 7] A band diagram is shown in Figure 3 to illustrate this point.

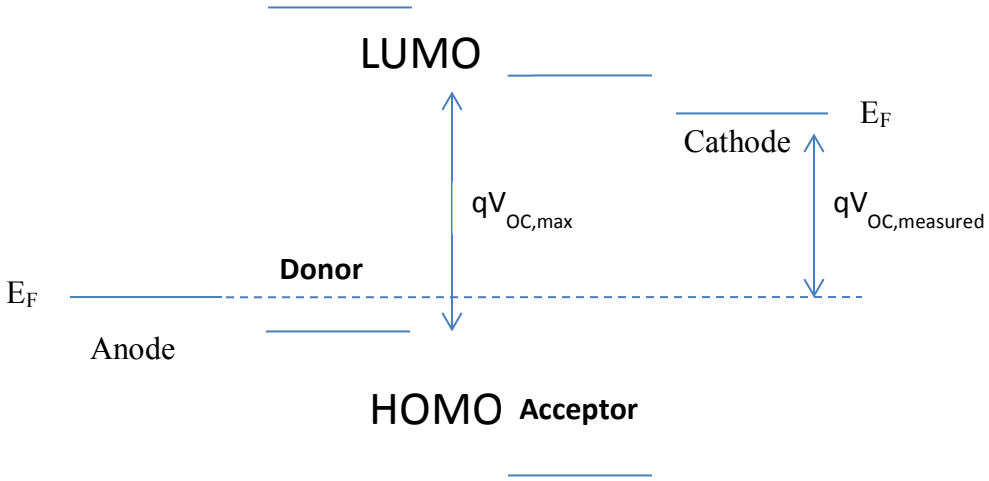

Figure 3: Open circuit voltage from a band diagram perspective.

Under open circuit voltage conditions excitons dissociate at the donor acceptor interface. The hole goes to the anode and the electron to the cathode. The cathode and anode are electrically isolated from each other leading to the term open circuit. A voltage is observed because of the fact under these conditions the excited electron is effectively 'trapped' in the cathode since there is no external mechanism for it to recombine with the hole in the anode. In a similar sense holes accrue at the anode and the separation of charge is what produces the potential difference observed, V_{OC}. The limitations of increasing V_{OC} include cost (if the cathode and anode were to have better energy level matching characteristics with the donor and acceptor materials they would in general become more expensive), opacity in the case of one of the electrodes, and reactivity of materials. Research is underway to modify the donor/acceptor interface with self-assembled monolayers (SAMs) in order to help adjust open circuit voltage (further discussed in section 2.3); this was one the focuses of this thesis.[10] Indium-doped tin oxide (ITO) was used as the transparent electrode because of its relatively low cost, optical transparency, and conductivity. The top electrode is typically silver or aluminum because they the materials are inexpensive though not optimal, in the sense that there are materials with better LUMO matching with the acceptor material; materials such as lithium and sodium which are rare and extremely reactive and thus would make devices expensive and have extremely limited lifetimes, respectively.[3,6,7]

2.2.2 Short Circuit Current

The short circuit current is defined as the current flowing in a cell under illumination through an external short circuit. Electrons will move toward the lower work function material while holes will drift toward the higher work function metal. This parameter is dependent on dissociation, charge collection, and absorption. These are many research groups working on some or all of these issues. One of the focuses of this thesis was to attempt to increase J_{SC} through dissociation and reduction of recombination using SAMs (further discussed in section 2.3).[6,10]

2.2.3 Fill Factor

Fill factor is defined as the maximum power generated by the cell divided by the product of the open circuit voltage and short circuit current. It describes the quality of the cell produced in that it can provide information about the amount of power lost while a cell is operating. A low FF (such as the straight line in Figure 4 where FF = 0.25) indicates an inefficient and poorly functioning cell and as the FF approaches the theoretical maximum of 1 the current-voltage curves is a step function at open circuit voltage short circuit current conditions. From a geometrical perspective FF is the ratio of the areas of rectangles(seen in Figure 4) of a cell operating at its maximum power point to its theoretical best. This is illustrated in Figure 4.

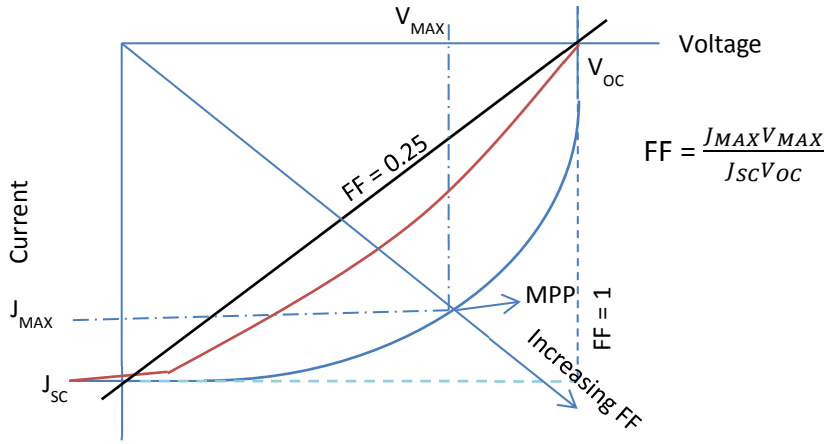

Figure 4: Current-voltage curves with curves of different fill factors. The open circuit voltage and short circuit current are indicated. The curve in the center represents a typical curve and FF would be calculated from the product of maximum current and maximum voltage divided by the product of open circuit voltage and short circuit current (MPP is maximum power point). The straight line indicates a FF of 0.25 while the dashed lines represent a FF of one (theoretical maximum).[2,6,7]

At this point it would be particularly instructive to view the solar cell from a circuit diagram perspective further discussed in section 2.2.4

2.2.4 Circuit Model of a Solar Cell

A useful and instructive way to understand the working of a solar cell can come from a simple equivalent circuit model of a solar cell which is shown in Figure 5.

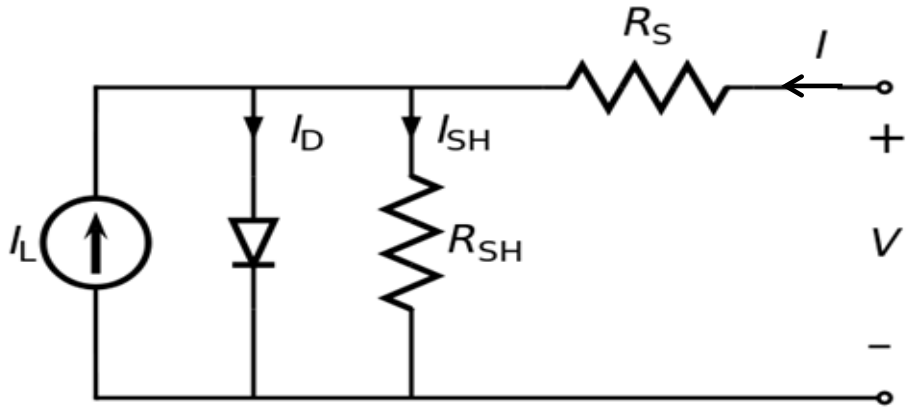

Figure 5: Equivalent circuit diagram of a solar cell. Adapted from the literature.[6]

The model above shows the open circuit voltage and short circuit current conditions. In the open circuit voltage situation there is no connection between the terminals at the terminal ends and under short circuit current conditions a dashed line representing a conducting wire with no resistance connected between the terminals. I_L, I_D, I_{SH}, and I are the photogenerated current, diode current (also known as dark current), shunt current, and overall output cell current respectively. Dark current is an important parameter that will be discussed further in depth in Chapter 4. R_{SH} and R_S represent the shunt and series resistances respectively.

Relating this model to Figure 4 it can be seen that a high series resistance should cause a smaller slope to around the open circuit voltage (the inverse of the slope gives resistance). A low shunt resistance, indicating charge carrier losses through processes such as shorting or recombination, is indicated by a large slope around the short circuit.

In this model open circuit voltage is

$$V_{OC} = \frac{nkT}{q} ln\left(\frac{I_L}{I_0} + 1\right) \qquad (1).$$

Where n is the diode ideality factor, q is elementary charge, T is temperature in Kelvin, k is Boltzmann's Constant and I_0 is the reverse saturation current. Short circuit current is roughly equal to the photogenerated current when the parallel resistance, R_{sh}, is large (because the current doesn't 'see' it as an avenue) .

This simple model allows is used for the cells tested in this thesis because it gives a good idea of where losses in a cell are occurring by providing an easy way to find shunt and series resistances. There are much more complicated models for thorough, in-depth analyses but for the purposes of this work the simple, single diode model is sufficient.

2.2.5 Efficiency

Efficiency is the ultimate judge of device feasibility in the 'real' world. It describes the ability of a cell to convert incident power from incoming light into electrical power. Equation 1 is the formula that is used to determine efficiency.

$$\eta = \frac{P_{max}}{P_{incident}} = \frac{J_{SC} V_{OC} FF}{P_{incident}} \qquad (2)$$

This is technically termed as the power conversion efficiency. It can be seen that all the aforementioned parameters play an equal and significant role in device efficiency. It is important to note that the efficiency has multiple components encapsulated in it such as efficiency of exciton dissociation, exciton recombination, charge extraction and negative effect of dark current, which reflects current passing through the diode, and not through the external circuit.

2.3 Self-Assembled Monolayers

Self assembled monolayers (SAMs) have been in used in applications as diverse as organic light emitting diodes, rust inhibitors, and biomedical devices.[11] In more recent years there have been successful attempts at using SAMs at the semiconductor-metal interfaces to improve charge collection in solar cells.[12] However, putting SAMs at the donor/acceptor interface of devices to prevent exciton recombination and modify the work function of materials, therefore potentially leading to higher J_{sc} and V_{OC} respectively, is still not well explored.

2.3.1 Bilayer Device Structure

The simplest device structure to analyze is the planar bilayer. In the course of this work the bilayer was composed of an inorganic acceptor, ZnO, and an organic donor, P3HT. This type of cell is known as a hybrid organic/inorganic solar cell and has been studied extensively.[2,3,5]

In a planar bilayer structure a donor and acceptor are sandwiched together between two electrodes, with the acceptor material being deposited on the transparent electrode. This is clearly shown in Figure 6.

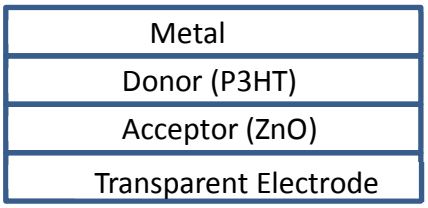

Figure 6: Bilayer device structure.

A band diagram of the above situation is illustrated in Figure 3. Through any material absorption of light is represented as a decaying exponential with increasing depth. This means that light is maximally absorbed when it first enters the cell. This first step determines exciton formation. In order for current to be produced the generated exciton

must be within a diffusion length, defined as the length an exciton can travel before recombining, away from the donor/acceptor interface. In thick layers (several times larger than the diffusion length) excitons may be generated that do not lead to current generation because they never reach the donor/acceptor interface and potentially dissociate. Planar bilayer devices in general suffer from this limitation since the absorber layer is at least an order of magnitude larger than the diffusion length therefore leading to a lack of dissociation. This design is not intended to maximize the interfacial area between donor and acceptor and is therefore not meant to give the best performing cells. The bilayer device structure was chosen for this thesis because of its simplicity of design and relative ease of analysis.[2,6,7]

2.3.2 Effects of SAMs at the Interface

As discussed previously there is significant room for improvement in terms of J_{SC} and V_{OC} for solar cell devices. One of the ways hypothesized to improve these parameters was through the use of SAMs.[10,12,13] In this thesis the P3HT/ZnO bilayer system was modified with several different types of SAMs and analyzed.

The use of SAMs provides a means to modify energy level offsets at the donor/acceptor interface and potentially offer a means to block excitons from recombining at trap states in the interface explained, this is explained further in Chapter 4. These SAMs can impart a dipole at the interface and therefore shift interfacial energy offsets which would affect the V_{OC}. This is shown in Figure 7.

A note on terminology is necessary. In organic vernacular, as explained previously, HOMO and LUMO are the terms used to describe energy levels. Their equivalents in the inorganic domain are valence band and conduction band respectively. This is why in the above diagram E_C and E_V are used where C denotes conduction band and V the valence band.

There are two reasons why SAMs may contribute to band offsets at the interface by means of dipoles. The first is the electron donating or accepting nature of the SAM. If it is an electron donor the dipole will point toward the donor and will shift its work function up therefore increasing V_{OC}. The opposite is true if the SAM is electron accepting. The second is the protonation of the metal oxide when a SAM has an acidic moiety. In this case there is a dissociative adsorption of the SAM in which there is a positive charge of a proton from the moiety on the SAM and a negative charge on the SAM itself.[10]

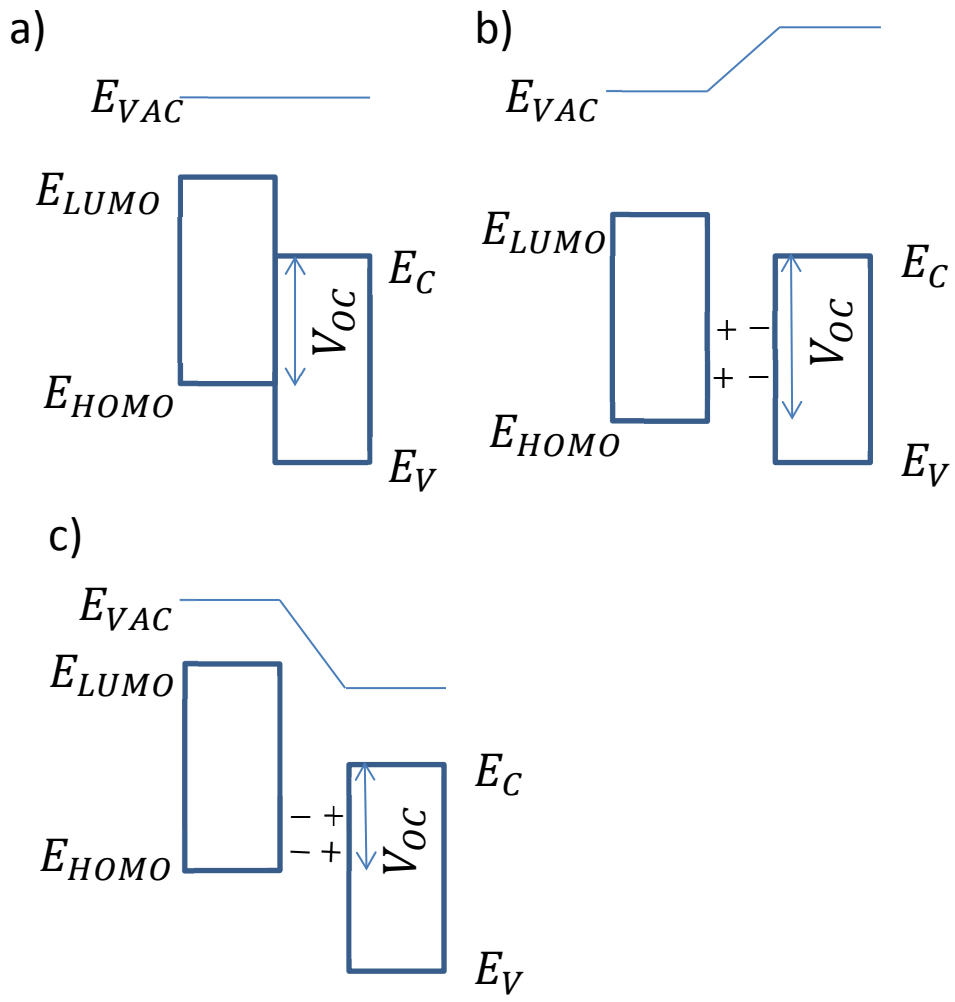

Figure 7: a) No SAM present between donor and acceptor. b) SAM with dipole pointing away from the acceptor. c) dipole pointing toward the acceptor.

SAMs' molecular orbitals at the interface provide electronic states which may reduce the probability of recombination and encourage charge transfer, for instance if the SAM were to accept an electron from the polymer. This can be seen in Figure 6 above. It is also known that SAMs passivate inorganic surfaces through reaction with surface dangling bonds, which are thought to provide recombination centres for excitons. Improvements in J_{SC} could be made for the aforementioned reasons.

2.4 Conclusions

In this chapter fundamental theory of OPVs was discussed. Semiconductor processes including absorption, excitation, diffusion, dissociation, and charge collection and transportation were discussed at length. Issues involved with these processes and what can be done to improve some of them. After that the key solar cell parameters of V_{OC}, J_{SC}, FF, and efficiency were explained. These parameters are fundamental in understanding the performance of device. An equivalent circuit model of a solar cell was introduced which is useful in understanding where losses could be occurring. Lastly the bilayer structure utilized in this thesis and the theory behind using SAMs to modify them was discussed.

CHAPTER 3 MATERIALS AND METHODS

The methods and materials involved in device fabrication and analysis will be discussed in the following sections.

3.1 DEVICE FABRICATION

SAM modified bilayer ZnO/P3HT devices are fabricated because they provide the clearest insight into the nature of hybrid devices. A diagram of the overall fabrication process is shown in Figure 8. Each fabrication step and the materials involved will be explained in detail in subsequent sections.

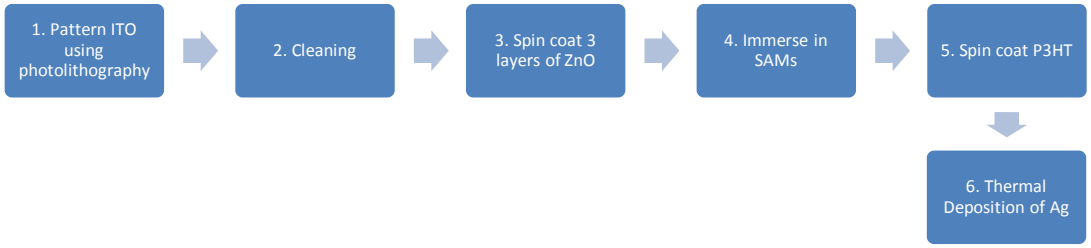

Figure 8: The overall fabrication process.

The first step in the fabrication process is to pattern the transparent conductive oxide, indium-doped tin oxide (ITO) purchased from Delta Technologies Limited, utilizing photolithography. This process allows for the fabrication of multiple devices on a single ITO substrate. The ITO is the electron collecting bottom electrode. The second step is cleaning ITO through a 20 minute sonication in each of the following solvents: acetone, deionized water and detergent, and deionized water (DI) alone. The water on the substrate is blown off using air. The final cleaning step is putting the patterned ITO in the reactive ion etcher (RIE) to remove any residual organics on the surface. The third step is

spin coating sol-gel synthesized ZnO onto ITO and subsequently annealing each of the three layers at 300°C.[14] This layer is the n-type electron accepting material in the device. The fourth step is the immersion of the coated substrate in a SAM solution for an optimized period of time. The fifth step is spin coating Poly(3-hexylthiophene-2,5-diyl) (P3HT), the electron donating layer purchased from Rieke Metals (BASF Sepiolid P200), on top of the ZnO. The substrate is then annealed at 140°C for 30 minutes in an Argon glovebox. The final stage of fabrication is the thermal deposition of the silver electrode. The devices are then tested using a solar simulator.

A fully fabricated device is shown in Figure 9 both with and without a SAM. The SAM layer is roughly on the scale of 1 nm in thickness if monolayer coverage is assumed.

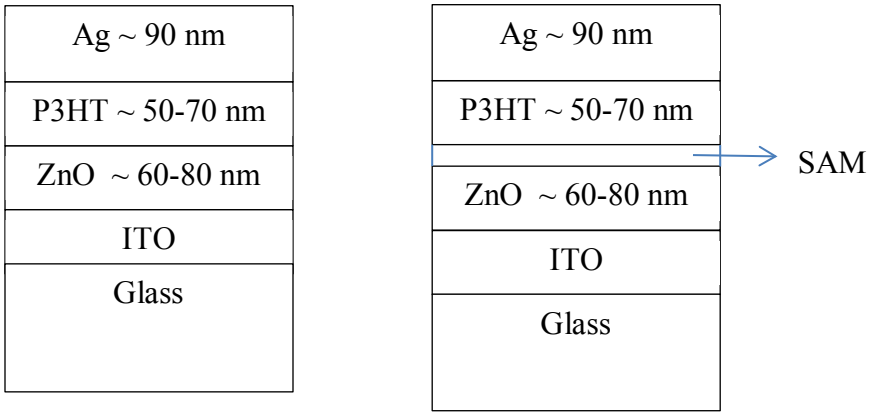

Figure 9: A side view of a fully fabricated device with and without a SAM

Light from the solar simulator is directed through the glass and ITO to the active ZnO/P3HT layers. The dimensions of a cell are 1 x 3 mm^2.

3.1.1 ITO

ITO is one of the most commonly used transparent conductive oxides chiefly because of its optical transparency and its conductivity. The ITO utilized throughout the project was purchased from Delta Technologies Limited and was prepared via sputtering onto alkaline earth boroaluminosilicate glass. Each of the substrates are 2.5 x 2.5 cm^2. It has

the following physical properties as specified by the manufacturer: 1) a sheet resistance of 15 – 25 Ω; 2) an ITO layer thickness between 80 and 120 nm; and 3) a transmittance greater than 78 %.

3.1.2 Photolithography

The Cobilt CA-800 Mask Aligner was used for the photolithographic process. The aligner is normally intended for the fabrication of micron-scale patterns on silicon wafers; however in the case of patterning ITO it acts as a convenient source of UV light.

3.1.3 ITO Patterning

A step by step diagram is shown in Figure 10 of the ITO patterning process. MEGAPOSIT™ SPR-220™ 3.0 photoresist was used as the etch mask without any further purification or modification. The procedure was adopted from SPR-220™ data sheet.[15]

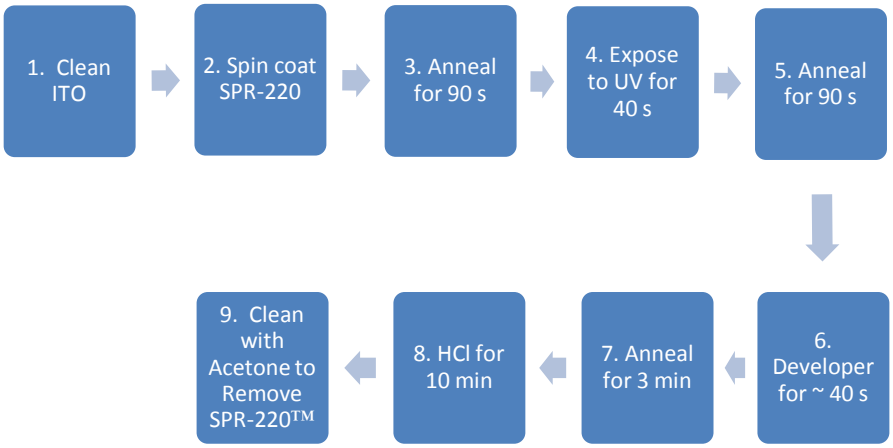

Figure 10: Step by step diagram of the ITO patterning process

The ITO is initially cleaned using a toothbrush and a DI/detergent mixture. The substrate is subsequently rinsed with DI and air is used to blow it off the surface afterwards. Afterwards SPR-220™ photoresist is spin-coated onto the ITO at 3000RPM for 40s to

yield a layer approximately 3.5 μm thick. The substrate is then annealed for 90s at approximately 120°C in air on a hotplate to remove residual solvent from the photoresist. The next step is to expose the parts which are desired to be etched to the UV source from the mask aligner for 40s. The areas of the photoresist that are exposed to the UV become susceptible to dissolution to the developer in step 6. After exposure to UV the substrate goes through its first hard bake for 90s to strengthen the unexposed photoresist. In the sixth step the substrate is immersed in MICROPOSIT™MF™-CD-26 developer to remove the parts of the polymer that were exposed during step 4; leaving the parts of the ITO that are desired to be etched exposed. The substrate is then rinsed with DI to remove any residual developer and blow dried before its put it is annealed for 3 minutes for its final hard bake. The eighth step is to submerge the substrate in HCl for approximately 10 minutes in order to etch the exposed ITO. Once the substrate is removed from HCl it is rinsed thoroughly with DI to ensure that there is no residual HCl on the substrate. The final step is to remove the photoresist by rinsing in acetone. A diagram of the lithographic process is shown in Figure 11.

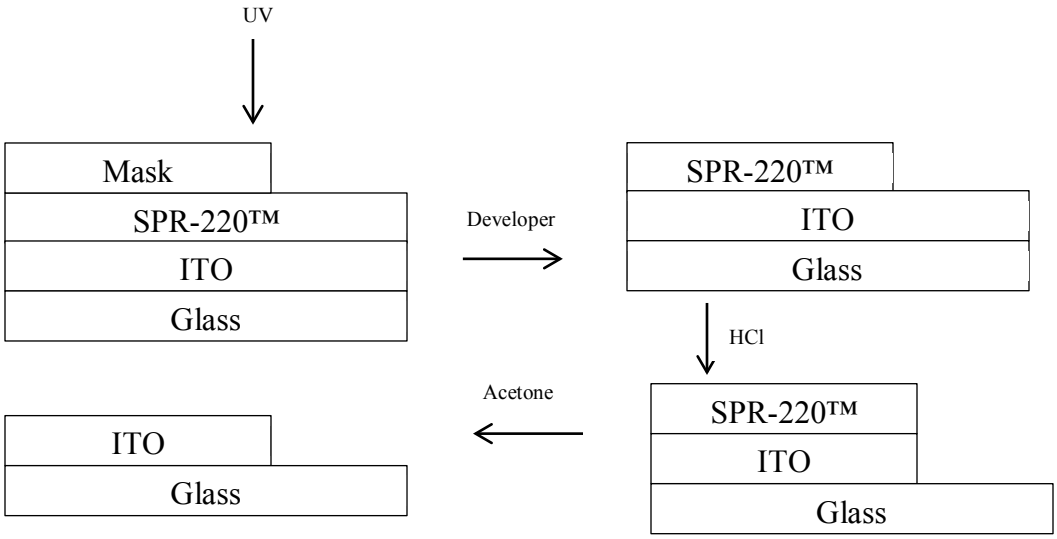

Figure 11: The complete photolithographic process.

The resulting strips of ITO are 1 x 12 mm^2, a top-down view of the layout is shown in Figure 12.

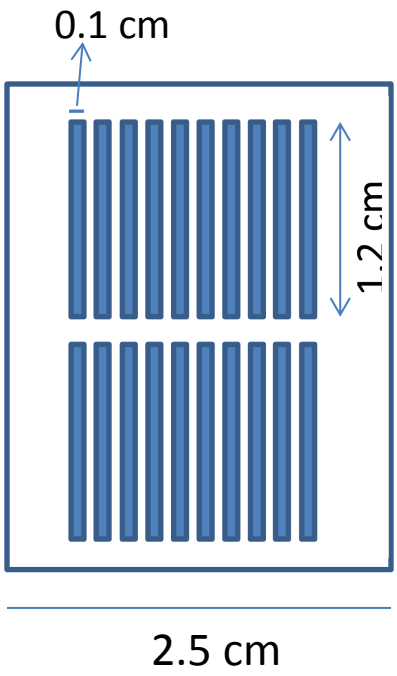

Figure 12: Top-down view of patterned ITO strips.

3.1.4 Spin Coating

The spin coater used was the Laurell Single Wafer Spin Processor Model WS- 400A-6NPP/LITE. Spin coating is a procedure in which a substrate is held in place on top of a rotor, with a solution (usually in a volatile solvent) placed on top, and spun. A uniform layer of material forms on the surface of the substrate as a result. The thickness of the material is roughly inversely proportional to the square root of the angular speed of the rotor and directly proportional to the viscosity and concentration of the fluid. A diagram of the spin coating process is shown in Figure 13.[16]

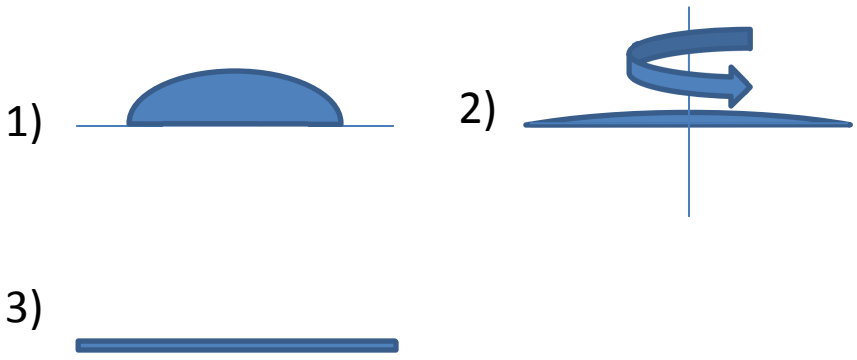

Figure 13: 1) a solution is applied to the substrate before spinning; 2) the substrate is spun at a certain angular speed; 3) a uniform layer is obtained.[16]

SPR-220 was spin-coated at 3000 rpm for 40 s as per the manufacturer's guidelines to give an approximately 3.50 µm layer. Sol gel ZnO was spin coated at 3000 rpm for 30 s as reported in the literature. P3HT was spin coated in a two step process: 1) 700 rpm for 1 minute; 2) 1000 rpm for 20 s. This procedure was based on previous literature and fabrication experience.[3,5,**Error! Bookmark not defined.**] The P3HT layer is approximately 50-70 m thick and this procedure was found to produce the most efficient cell. This is likely due to that fact that of the different spin procedures used those that gave too thick of a layer inhibited hole transport to the anode and those were too thin a layer did not absorb an optimal amount of the incoming light and hampering maximal exciton formation.

3.1.5 Sonication

The sonication apparatus utilized was the 2510 Branson Sonicator. A transducer produces alternating high and low pressure regions in liquid causing bubbles to form and then burst through cavitation. Substrates are often put in a solvent and then sonicated to remove dirt and grime because of the relatively intense nature of the cleaning process.[17]

3.1.6 Reactive Ion Etching

A parallel plate reactive ion etcher (RIE) was utilized in the course of this work, the Phantom II. The RIE is a complex instrument and the details of its operation and the interactions of free ions with a substrate are given elsewhere.[18] A brief treatment shall be given here.

In a parallel plate RIE a field is applied between two plates at a radio frequency (RF) of approximately 13.56 MHz.[19,20] A gas is then let into the chamber, in the case of this work oxygen, and a certain power is applied and plasma is generated. This oxygen plasma is composed of highly reactive ions which bind to organic contaminants on the surface readily. The products of this reaction are gaseous and removed via vacuum. A schematic diagram is shown of the process in Figure 14.

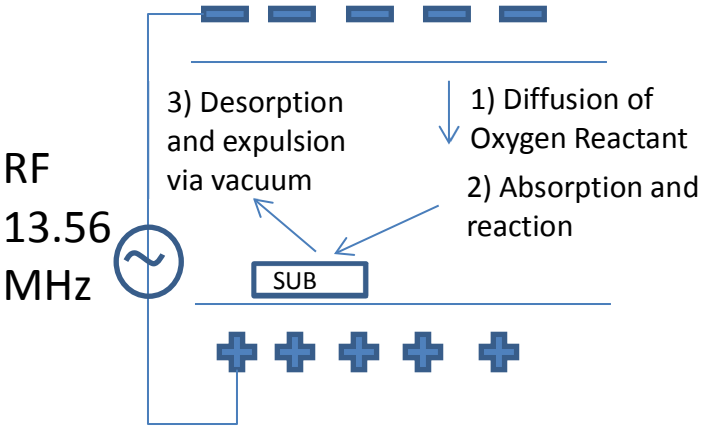

Figure 14: RIE reaction processes.

3.1.7 ZnO Preparation

The ZnO acceptor material used was prepared using a procedure found in the literature. Zinc acetate dehydrate ($ZnAc \cdot 2H_2O$) was dissolved in 2-methoxyethanol and monoethanolamine (MEA) at room temperature in a round bottom flask up until the

$ZnAc{\cdot}2H_2O$ was completely dissolved and then the solution was heated to approximately 60°C for 2 hours. The molar ratio of MEA to $ZnAc{\cdot}2H_2O$ was 1 and the concentration of $ZnAc{\cdot}2H_2O$ was 0.35 M.[14]

An SEM image of ZnO on an ITO substrate is shown in Figure 15.

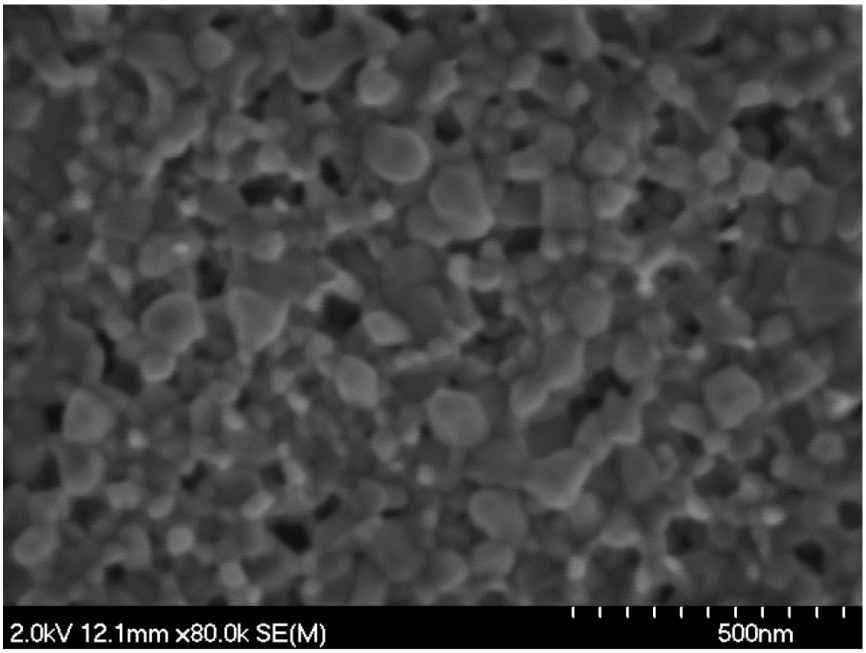

Figure 15: SEM image of ZnO on an ITO substrate

It can be seen from the image that the ZnO nanoparticles are roughly 30 nm in diameter and are distributed unevenly across the surface.

3.1.8 Self-assembled Monolayers

A 1 mM solution of a SAMs was prepared using acetonitrile (anhydrous) and ethanol (anhydrous) as solvents. The ZnO covered substrates were immersed for an optimized period of time in the SAM solution. The benzoic acid SAMs were purchased from Fisher Scientific and they were: benzoic acid (99% Cat. No. A65-500), 4-aminobenzoic acid (99% Cat. No. AC14621-0010), 4-methoxybenzoic acid (98% Cat. No. AC15237-1000),

and 4-cyanobenzoic acid (99% Cat. No. AC11073-0250). The phenylphosphonic acid SAMs were purchased from Sigma Aldrich and they were: phenylphosphonic acid (98% Cat. No. P29006). Immersion times and molecular structures will be introduced and further discussed in Chapter 4.

3.1.9 P3HT

A 20 mg/mL solution of P3HT donor material was prepared in 1,2-diclorobenzene under argon.[2,3] The solution was left stirring at 60°C for 12 hours, to ensure complete dissolution, before use. P3HT was used as purchased from Rieke Metals with a regioregularity of 95%, a molecular weight of 20-30K, and a field effect hole mobility of 0.3 $\frac{cm^2}{V\,s}$. The chemical structure is shown in Figure 16.

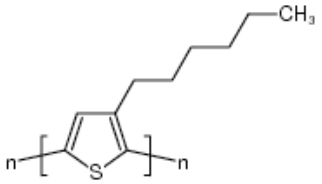

Figure 16: P3HT

3.1.10 Bell Jar Thermal Evaporation System

To deposit the silver electrode a bell jar thermal evaporation system was used. A simplified description will be given here of its operation. The bell jar system achieves vacuum pressures as low as 1 x 10^{-6} Torr which correlates to a mean free path of approximately 7.7 m for silver as calculated by Equation 2.

$$\lambda = \frac{RT}{\sqrt{2}\pi P N_A d^2} \quad (2)$$

Where R is the universal gas constant, T is temperature, P is pressure, d is the diameter of the particle, N_A is Avagrado's number, and λ is the mean free path. This is important because the mean free path should be at least the same length as the bell jar height, which is 40 cm, in order to guarantee that silver particles evaporate onto the substrate in a uniform manner. So in the case of the bell jar system in use the pressure is lower than adequate for a uniform deposition to take place. It is important to keep in mind Equation (1) provides only a rough estimation of the mean free path.[21] Once a low enough pressure has been achieved the deposition process can begin.

Silver, 99.99% pure, pellets were used as purchased from Kurt J. Lesker. The silver is first melted in a tungsten basket, while a pair of shutters covers the substrate, until the rate of deposition is approximately 1 Å/s as measured by a Sycon Thickness Monitor (STM). The shutters are then opened until approximately 90 nm of silver has been deposited onto the substrate, at which point the shutters are closed and the system is shut down.

3.1.11 Clean Room

With the exception of silver deposition, all processes were performed in a Terra Universal class 1000 clean room, which optimaly has a maximum of 1000 particles of diameters greater than or equal to 0.5 μm, per ft^3. Processes were performed in the clean room to prevent dust from accumulating on devices and inhibiting performance.

3.2 ANALYSIS TECHNIQUES

The solar simulator system is discussed in the following section. A current-voltage curve was generated for each cell and the following parameters were obtained: open circuit voltage, short circuit current, fill factor, and efficiency.

3.2.1 Solar Simulator System

To test fabricated devices a setup with a 150-watt Oriel Solar Simulator from Newport with a xenon lamp, two Signatone probes, a Keithley 236 Source Measurement Unit (SMU), a steel probe platform was utilized, and a Thor Labs power meter. The lamp outputs roughly the same spectrum as the sun but was further modified with AM0 and AM1.5 Direct filters. The AM0 filter was used to adjust the spectrum to what it would be just outside Earth's atmosphere. The AM1.5 filter further adjusted the spectrum so it would match what it would be if the sun were to pass through 1.5 atmospheres. The beam intensity is variable with beam collimation because of the intensity of the xenon arc lamp. A power meter was used to calibrate the output beam (measured in $\frac{W}{m^2}$). In Figure 17 the accepted AM1.5 solar irradiance and the scaled solar irradiance from simulator are plotted.[7]

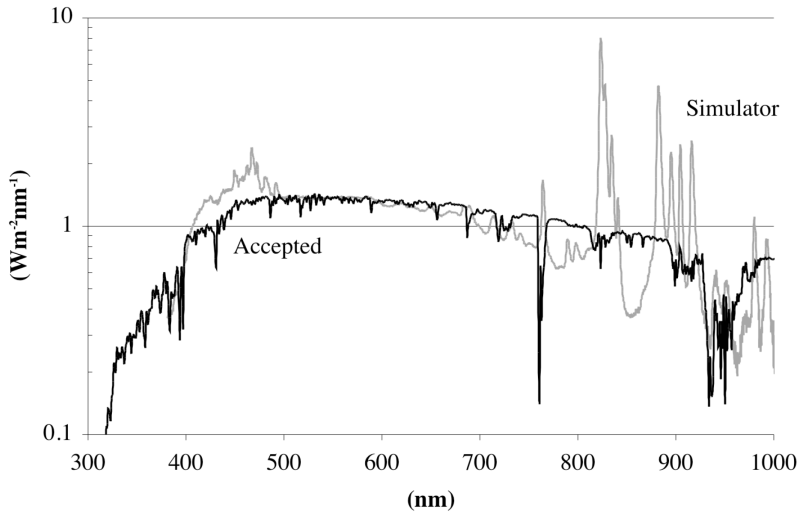

Figure 17: The accepted AM1.5 solar irradiance and the scaled simulator irradiance.[7]

The peaks in the simulated solar irradiance stem (in the spectrum between 800-900 nm) from the use of the xenon arc lamp.

The cell was tested on the probe station with one probe contacting ITO and the other silver. The Signatone probes were also connected to the SMU and labview code was run

to do a current-voltage sweep on each device. All cells were tested in air under ambient conditions.

3.2.2 Kelvin Probe

A Kelvin probe, from KP technology, was used to take measurements of contact potential differences (CPD). These measurements allowed for the determination of relative work function changes between ZnO and SAM modified ZnO on ITO substrates.

In a Kelvin Probe a flat, circular, vibrating reference electrode is suspended over the sample, which acts as stationary electrode, thus forming a capacitor. To fully illustrate and understand how these measurements are made it is necessary to see Figure 17.

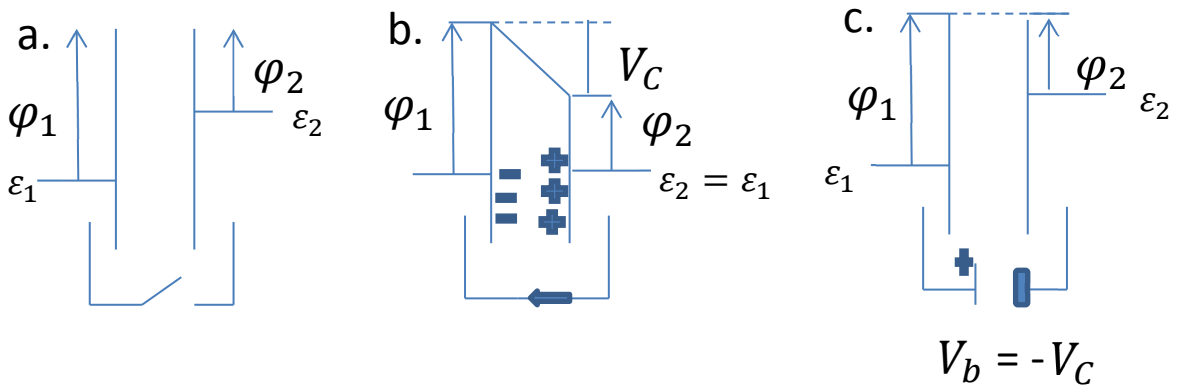

Figure 18: a. Two electrically isolated but conducting samples with work functions φ_1 and φ_2 and Fermi energies ε_1 and ε_2. b. If an electrical connection is made between the two materials the Fermi energies equalize and charge flows in the direction indicated, producing a potential gradient known as the contact potential V_C between the two materials. The two surfaces are equally but oppositely charged. c. A variable backing potential V_b is applied to one electrode and when $V_b = -V_C$ the electric field between the surfaces vanishes and a null output signal is produced.[22]

In a. it can be seen that there are two electrically isolated but conducting samples with work functions φ_1 and φ_2 and Fermi energies ε_1 and ε_2. At b. it is seen that if an electrical connection is made between the two materials the Fermi energies equalize and electrons flow in the direction indicated, producing a potential gradient known as the contact potential V_C between the two materials. As a result the two surfaces are equally but oppositely charged. In c. a variable backing potential V_b is applied to one electrode and when $V_b = - V_C$ the electric field between the surfaces vanishes and a null output signal is produced.

In the Kelvin probe apparatus a vibrating tip (acting like a capacitor) hovers over the surface of a conductive sample. The apparatus detects minute changes in current flow. A series of capacitances is then calculated according to equation (3) based on the varying distances between the vibrating tip and sample.

$$C = \frac{A\epsilon_0}{d} \qquad (3)$$

where C is capacitance, A is the area of overlap between the two surfaces, ϵ_0 is the electric constant, and d is the separation distance. The point where there is no longer current flow is then found and is termed the contact potential difference (CPD) which is actually $-V_b$ as shown in Figure 17 c. Equation (3) gives a clearer picture of what is occurring

$$\frac{dQ}{dt} = I = \frac{d}{dt}(CV) = V\frac{dC}{dt}\Big|_{const\ V} \quad (4)$$

where Q is charge, t is time, I is current, and V is voltage. In a Kelvin probe voltage is applied and current is measured.

A vibrating tip utilizes a lock-in amplifier to monitor AC current produced. To maintain electric field between surfaces the amount of charge varies due to the vibrating tips constantly changing distances from the sample. A vibrating tip is used to collect many

data points because of the varying distances and then a current-voltage curve is fitted and the zero current point is determined. That is how work function changes are detected with a Kelvin probe.[22,23]

Measurements are extremely sensitive to environmental factors such as noise, vibration, humidity, etc. As a result measurements on multiple samples were always performed on the same day. All measurements were in made mV.

3.2.3 Contact Angle

Contact Angle measurements were made using a First Ten Angstroms (FTA) contact angle goniometer. Essentially it is a composed of a stage on which the sample sits and a camera to take a picture of a drop that is deposited on the surface of the sample (in the case of this work the drop was water). Once a picture was taken FTA software was used to determine contact angle. Contact angle measurements provided information about the level of SAM coverage on ZnO.

Contact angle quantifies the wettability of a solid surface and is technically defined as where the vapor/liquid interface physically interacts with a solid surface. A unique contact angle is observed for a given system of solid, liquid, and vapor at a fixed temperature and pressure. When measured at equilibrium conditions the contact angle provides information about the relative strength of the liquid, solid, and vapor molecular interactions.[24,25] In this dissertation deionized water, which is polar, was used as the liquid sessile drop on the surface. All the SAMs used had a nonpolar base benzene ring so it was expected that if the SAM adhered well to the surface there should be a relatively high contact angle as compared to water on bare ZnO (expected to be polar because of hydroxyl groups on the surface) which was measured to be 16°. This expectation stems from the oft cited chemistry rule that like dissolves like (e.g. polar dissolves polar, non-polar dissolves non-polar). A contact angle measurement is illustrated in Figure 19.

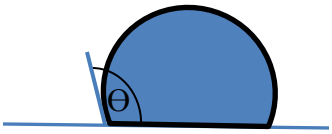

Figure 19: Contact angle Θ of a liquid on a solid substrate.

3.3 CONCLUSIONS

The process of fabricating a cell and the techniques associated with its analysis has been described in this chapter. The following chapter will be presenting and discussing the data collected from the contact angle goniometer, Kelvin probe, and solar simulator.

CHAPTER 4 RESULTS AND DISCUSSION

4.1 Contact Angle Measurements

Contact Angle measurements were performed on SAM modified ZnO substrates as a function of immersion time to determine the optimal coverage of the sample. Contact angle measurements on bare ZnO yielded a value of 16° and this value was used a benchmark to compare with SAM immersed samples. Benzoic acid and phenyl phosphonic acid derivatives were used as SAMs based on previous research on their use in other metal oxides such as TiO_2.[10,11,12] It is important to note that there is approximately ±0.5° of variation for each sample. Error bars were not included in the graphs because the sample size was not large enough to make a statistically valid statement on error (there were four samples for each data point). Values are compared with those in the literature where information is available.

4.1.1 Benzoic Acid Derivatives

The results of contact angle measurements over time for benzoic acid, 4-methoxybenxoic acid, 4-aminobenzoic acid, and 4-cyanobenzoic acid are shown in the Figures 20 to 23 with corresponding chemical structures. All of the benzoic acid derivatives were dissolved in anhydrous acetonitrile at 1 mM concentrations.

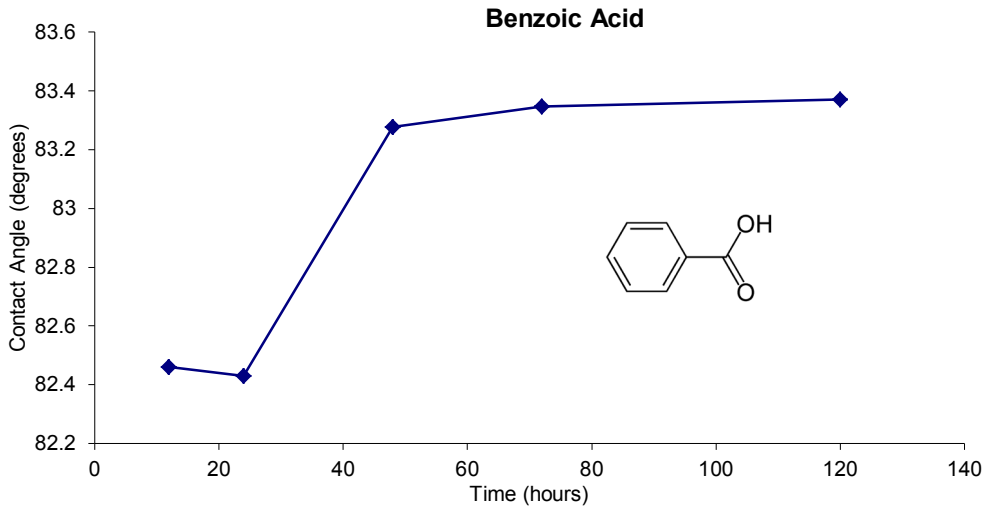

Figure 20: Substrates immersed in benzoic acid over a 120 hour period.

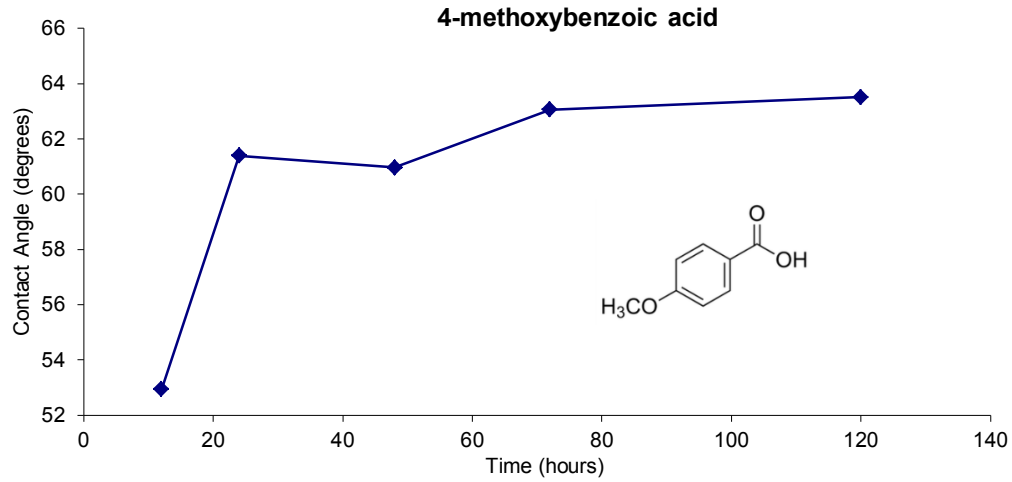

Figure 21: Substrates immersed in 4-methoxybenzoic acid over a 120 hour period.

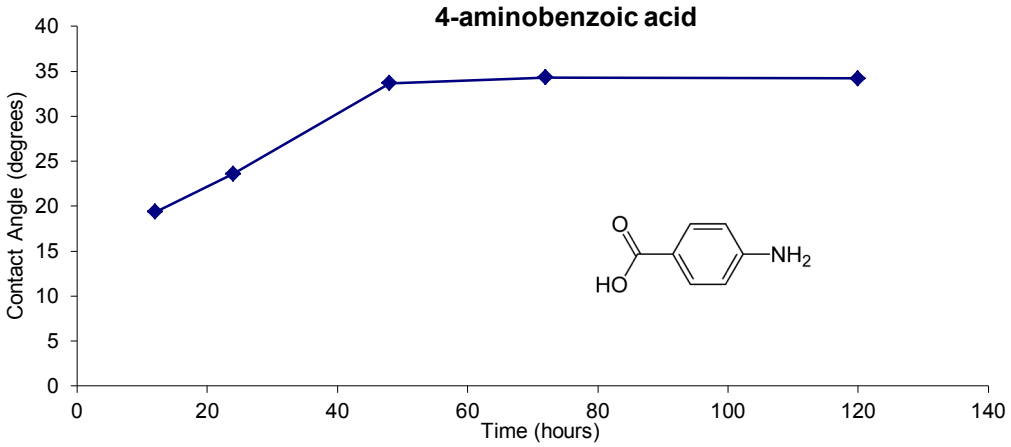

Figure 22: Substrates immersed in 4-aminobenzoic acid over a 120 hour period.

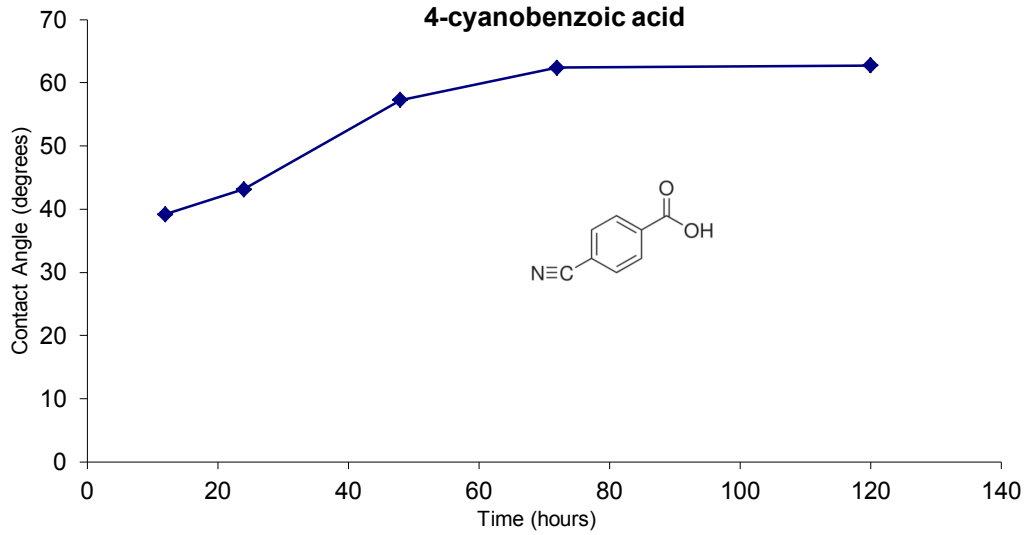

Figure 23: Substrates immersed in 4-cyanobenzoic acid over a 120 hour period.

The optimal immersion time for all benzoic acid derivatives was determined to be approximately 72 hours. The ultimate contact angle values for benzoic acid, 4-methoxy benzoic acid, 4-aminobenzoic acid, and 4-cyanobenzoic acid were determined to be 83, 64, 34, and 63 degrees respectively.

4.1.2 Phenyl Phosphonic Acid Derivatives

The results of contact angle measurements over time for phenylphosphonic acid and 4-methoxyphenylphosphonic acid shown in Figures 24 and 25 with corresponding chemical structures. Both SAMs were dissolved in anhydrous ethanol at 1 mM concentrations.

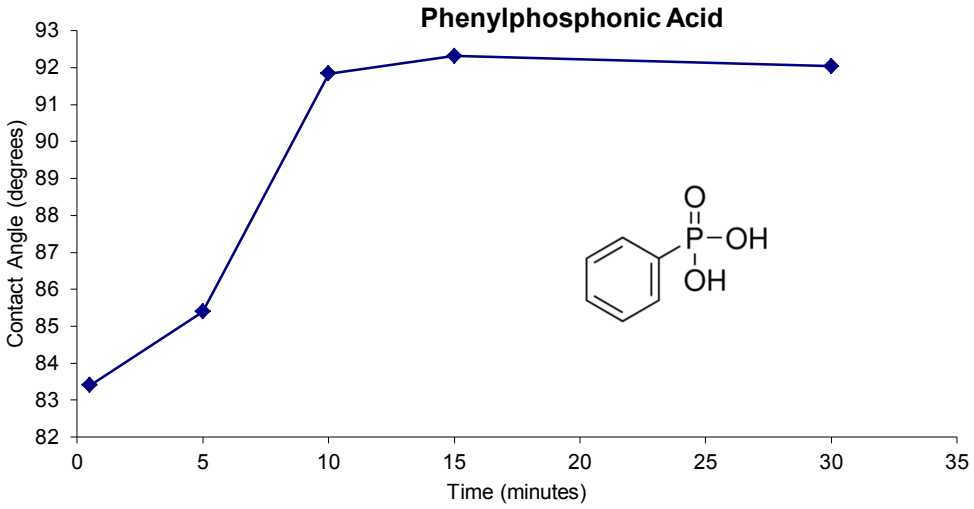

Figure 24: Substrates immersed in phenylphosphonic acid over a 30 minute period.

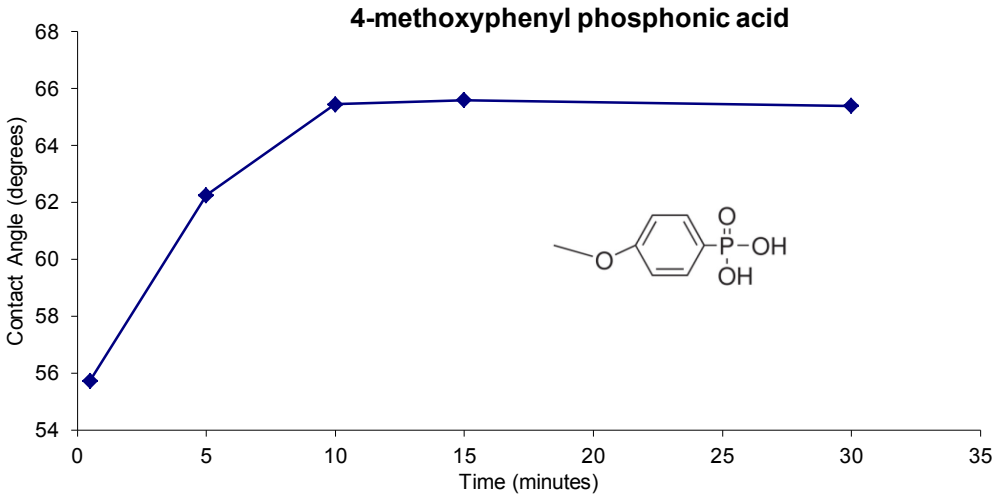

Figure 25: Substrates immersed in 4-methoxyphenylphosphonic acid over a 30 minute period.

The optimal immersion time was determined to be approximately 15 minutes. The ultimate contact angle values achieved for phenylphosphonic acid and 4-methoxyphenylphosphonic acid were 92 and 65 degrees respectively.

4.1.3 Discussion

Table 1 shows all the measured contact angle values versus those obtained in the literature.[26] It is important to note the SAMs in the literature were grown on TiO_2 and because of the similar chemical nature of metal oxide behaviours it provides a good basis for comparison since it is likely that the SAMs used binds chemically to the surface of ZnO in a similar fashion. All SAMs in theory should be binding to the ZnO with their respective acidic functional group.

Table 1: Contact angles of the benzoic and phenylphosphonic acid derivatives compared to the literature. All values are in degrees

SAM	**Contact Angle ±0.5 (meas.)**	**Contact Angle (lit.)**
Benzoic acid	83	77
4-methoxybenzoic acid	64	60
4-aminobenzoic acid	34	44
4-cyanobenzoic acid	63	38
Phenylphosphonic acid	92	(see benzoic acid)
4-methoxyphenylphosphonic acid	65	(see 4-methoxybenzoic acid)

It can be seen that except in the case of 4-cyanobenzoic acid, there is relatively good agreement between the measured values and those reported in the literature. It would also be reasonable to compare the phenylphosphonic acid derivatives to the benzoic acid derivatives because of the similar chemical nature of the non-binding benzene and associated functional groups.

Of the contact angles measured the SAMs with a plain benzene ring, benzoic acid and phenylphosphonic acid, exhibit the highest contact angles. This is because of the non-polar nature of the benzene group which makes the surface relatively hydrophobic. A plausible reason for the difference in contact angle between the phenylphosphonic acid and benzoic acid could stem from the fact that benzoic acid was not completely adhered to the surface of the substrate. The benzoic acid molecules could be oriented in different directions on the substrate surface. For instance some molecules might have the carboxylic acid group (polar) facing away from the surface making the surface more hydrophilic.[10,11,12]

The other functional groups on the benzene ring (regardless of acidic group) lead to lower contact angle values as compared with their plain benzene counterparts. The reasons for this could be due to the more polar nature of the functional groups, or the improper adherence of the SAM to the surface in the sense that molecules could be oriented in other ways than having their acidic binding group facing and reacting with ZnO, both of these reasons combined, or some sort of alternate chemical reaction involving the functional group with the drop of water used to determine contact angle.[10,11]

The molecules are presented in order of decreasing polarity, and therefore what should be in increasing contact angle, in Table 1: 4-cyanobenzoic acid, 4-methoxybenzoic acid, 4-aminobenzoic acid, and benzoic acid. If polarity alone were the determining factor it would be expected that contact angles should be observed to be increasing. Experimentally this is almost precisely what is observed. Ordered in terms of increasing contact angle is: 4-aminobenzoic acid, 4-cyanobenzoic acid, 4-methoxybenzoic acid, and benzoic acid.[10] The SAM that does not completely fit this picture is the 4-aminobenzoic acid. As stated before it may be due to different orientations of the SAM on the substrate or it could be due to the basic nature of the amino group which could be reacting with the sessile drop of water on the surface used to determine contact angle.

There are a variety of complex chemical and physical factors governing how SAMs attach to the substrate surface. Considerations such as the geometry of the molecule and the interactions of neighboring functional groups could push them to orient in ways other than the preferred orientation of acid facing and reacting with the ZnO substrate. It was beyond the scope of this work to go into a detailed study of these effects.

It is interesting to note the difference in immersion times between the phenylphosphonic acids and the benzoic acids. The reason is likely because of the chemical reactivity of the phosphonic acids as compared to their benzoic acid counterparts which makes their SAM growth occur on the order of minutes versus days. [10,11 ,27]

4.2 Kelvin Probe Measurements

Contact potential difference (CPDs) measurements were performed using a Kelvin probe in ambient conditions. Measurements were made on benzoic and phenylphosphonic acid covered ZnO on ITO, using plain ZnO on ITO as the reference. Measurements on respective acid groups were performed on the same day to ensure consistent results. CPDs were plotted against dipole moments in Debyes. Dipole moments were obtained from the literature where they were calculated using density functional theory in Gaussian. It should be noted that calculations only looked at the benzene ring and associated functional groups without the acid group or the substrate. This can be justified because CPD comparisons are being made relative to the same, plain benzoic acid molecule, so an absolutely correct simulation for the determination of dipole moment would not be necessary as it would yield the same comparative differences.[10,26] Where data is available results are compared to those in the literature.

4.2.1 Benzoic Acid Derivatives

In Figure 26 CPDs plotted against dipole moments in Debyes for 4-methoxybenzoic acid (MBA), 4-aminobenzoic acid (ABA), benzoic acid (BA), and 4-cyanobenzoic acid (CBA) are presented.

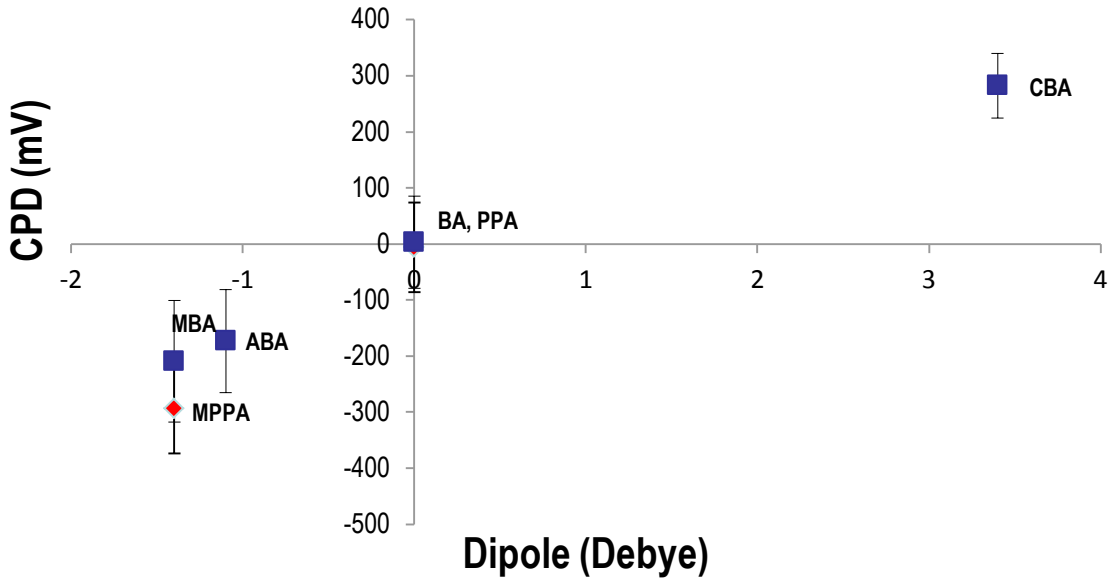

Figure 26: Benzoic acid derivatives CPD relative to bare ZnO versus dipole moment with a dashed guide line.

As can be seen there is a linear trend. The molecules with the dipole directed away from the ZnO decrease its work function by 170 mV and 210 mV for ABA and MBA respectively so that a situation akin to Figure 6 b) has occurred. It can be seen that BA has almost no effect on CPD and an energy level diagram in Figure 6 a) best depicts this situation. CBA has the opposite effect on the state of energy levels, decreasing work function by 280 mV, and its state is depicted in Figure 6 c). More will be discussed on the effect of these SAMs (excepting CBA) on the donor-acceptor interface in section 2.3. These molecules were selected because of previous studies of the SAMs on TiO_2 in the literature.[10,28] Comparisons with literature values will be made in the discussion section.

4.2.2 Phenylphosphonic Acid Derivatives

SAMs of phenylphosphonic acid (PPA) and 4-methoxyphenylphosphonic acid (MPPA) on ZnO were analyzed using the Kelvin probe. These two molecules were selected because of the nature of their phosphonic acid anchoring group which is thought to be a more effective anchoring group than their benzoic acid counterparts. [10,11] Figure 26 shows CPD versus dipole moment of the two SAMs.

As can be seen there is similar behavior between the phenylphosphonic acids and benzoic acids which is not that surprising if the acid groups on the ends are doing nothing more than anchoring these molecules to the surface of ZnO. As stated in the previous sub section the energy level diagrams are best represented by Figure 6 a) and b) for PPA and MPPA respectively. The measured CPD, as compared to ZnO, for MPPA was -290 mV and for PPA was -1 mV.

4.2.3 Discussion

Table shows the measured CPD values and those found in the literature.[28]

Table 2: CPDs of measured and literature values

SAM	**CPD (mV) (meas.) ± 50**	**CPD (mV) (lit.)**
BA	3	-10
MBA	-210	-220
ABA	-170	---
CBA	280	1000
PPA	-290	---
MPPA	-6	---

As can be seen from Table 2 the CPDs match fairly closely with those found in the literature with the exception of CBA. There could be a variety of reasons but perhaps the

most likely may have to with the purity of the CBA used or with the poor SAM formation on the substrate.

4.3 Current-Voltage Curves

Current-voltage (J-V) curves are arguably the most important judge of cell function and performance. The parameters of V_{OC}, J_{SC}, FF, and efficiency are determined from these curves and an understanding of the cells can be gleaned from these parameters. In this section J-V data for benzoic acid and phenylphosphonic acid derivatives will be presented and discussed. All cells are compared to a standard, unmodified planar bilayer ZnO/P3HT cell. Before proceeding dark current and its use as an indicator of what is occurring in terms of exciton recombination at the donor/acceptor interface must be explained.

Dark current, alternatively named the diode current, refers to the current generated while the cell is not under illumination. An energy level diagram of this situation is shown in Figure 27.

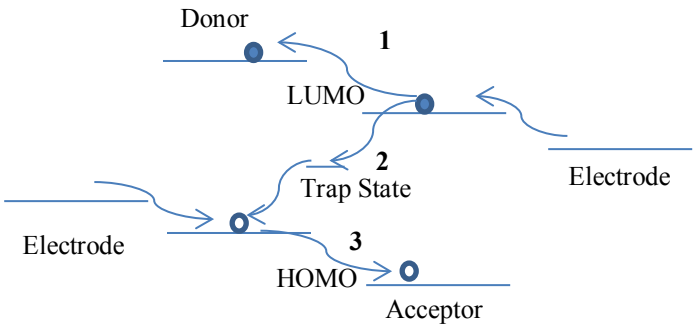

Figure 27: Energy level diagram in dark current conditions. In process **1** the electron moves from the acceptor LUMO and to donor LUMO without 'seeing' the trap state. In process **2** the electron goes to the lower energy trap state and recombines with the hole in the donor's HOMO. This is the process predominantly responsible for the observed dark current. In process **3** the hole from the donor's HOMO jumps to the acceptor's HOMO.

If the difference in HOMO-HOMO and LUMO-LUMO energies is sufficiently large processes **1** and **3** will not occur only **2**. Process **2** is the predominant reason for observed dark current and SAMs may offer a solution. The reason why dark current offers a strong clue as to what is going on at the donor/acceptor interface when SAMs are utilized, which are supposed to decrease exciton recombination are utilized, is best shown using Figure 28.

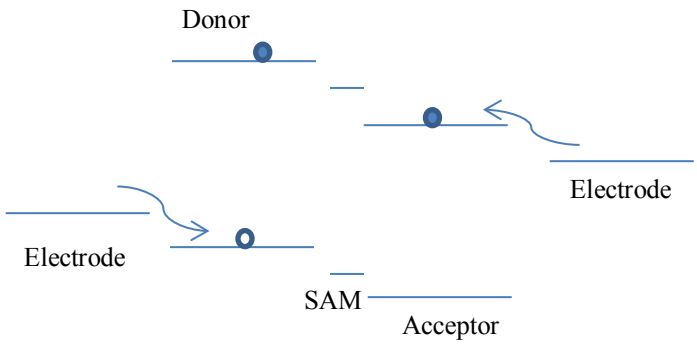

Figure 28: Dark conditions with a SAM at the donor/acceptor interface.

As can be observed from Figure 28 a SAM with energy level characteristics where the electron has to overcome an energy barrier to reach the acceptor and where there is an energy level between the LUMO of the donor and LUMO of acceptor is the ideal case. This kind of SAM inhibits recombination under illumination because there is a relatively large energy barrier preventing recombination (see Figure 39) with the hole in the donor material stopping process **2** in Figure 27 from occurring. This physical separation and the passivation of ZnO substrate are responsible for decreases in dark current from SAMs. In the following sections, with the SAMs used in this dissertation, it will be seen that this kind of electronic level structure was unlikely to have been forming but the SAMs may still offer hints as to the kinds of molecules that should be used.

4.3.1 Unmodified ZnO/P3HT Devices

Unmodified ZnO/P3HT devices' illuminated current-voltage curves respectively are shown in Figure 29. Multiple curves are shown from different devices and are indicative of the uniformity of operational cells on a substrate. Dark curves were not included because of the fact they overlap so closely (see solid line in Figure 30 for an example of a P3HT/ZnO dark curve).

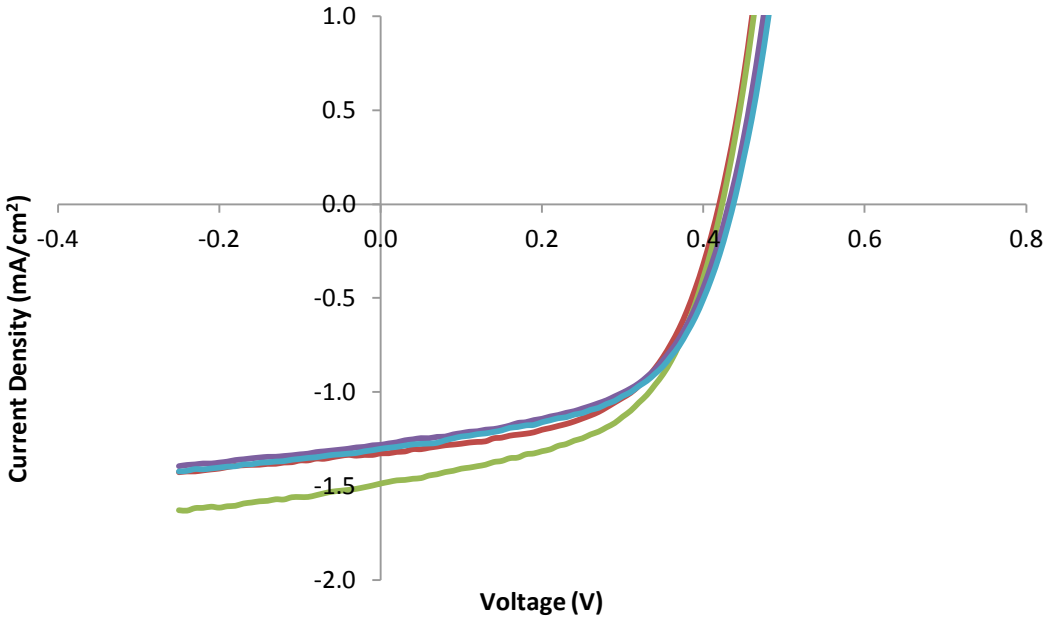

Figure 29: Multiple current-voltage curves from differing unmodified ZnO/P3HT devices.

4.3.2 Benzoic Acid Derivatives

Presented here will be BA, MBA, and ABA cells under dark and illuminated conditions. The dark curves provide information about the dark current which reflects the status of recombination at the donor/acceptor interface. A decrease in dark current reflects a decrease in recombination and an increase would the opposite. CBA was excluded because it produced malfunctioning devices for reasons that will be explained in section

4.3.3. The dark and illuminated curves for BA are shown in Figures 30 and 31 where J is current density. They are plotted as compared to a standard ZnO/P3HT cell.

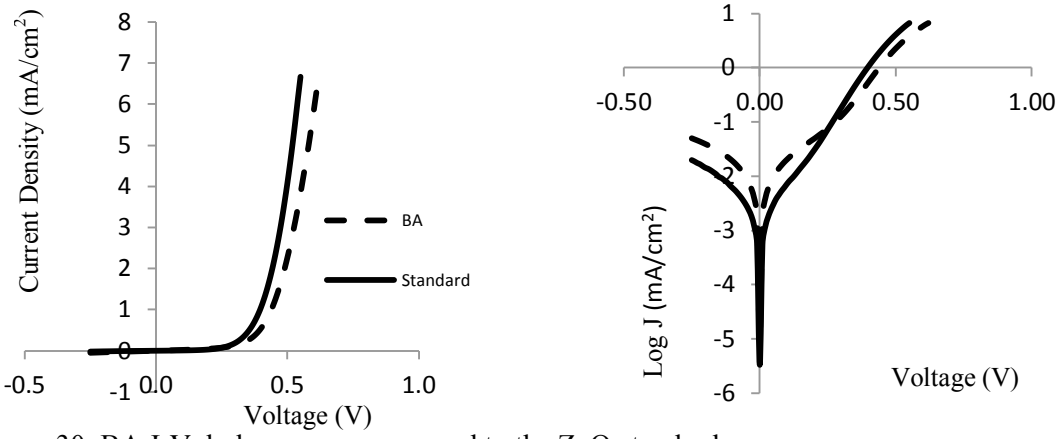

Figure 30: BA J-V dark curve as compared to the ZnO standard.

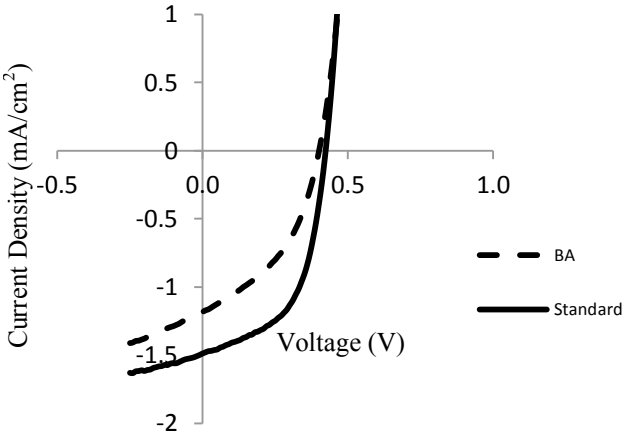

Figure 31: BA illuminated J-V curves as compared to ZnO standard

Figures 32 and 33 show MBA cells under dark and illuminated conditions, respectively.

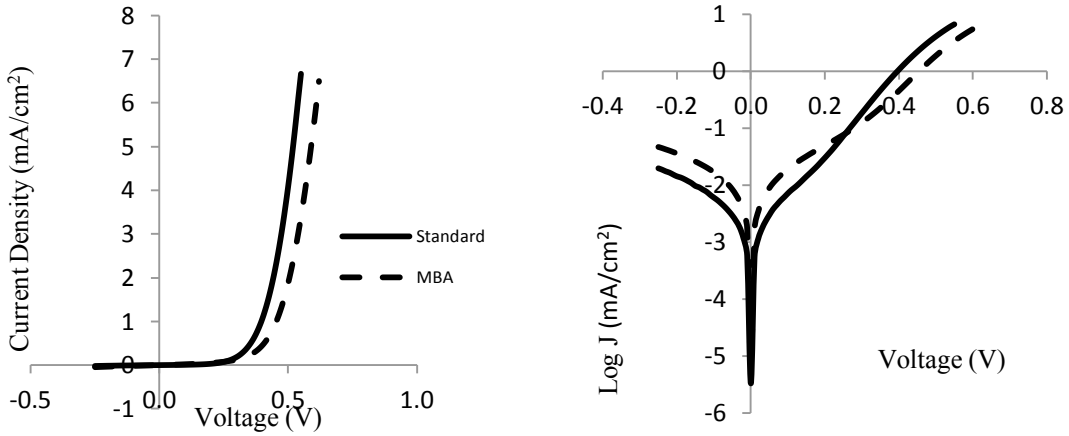

Figure 32: MBA J-V dark curve compared to ZnO standard.

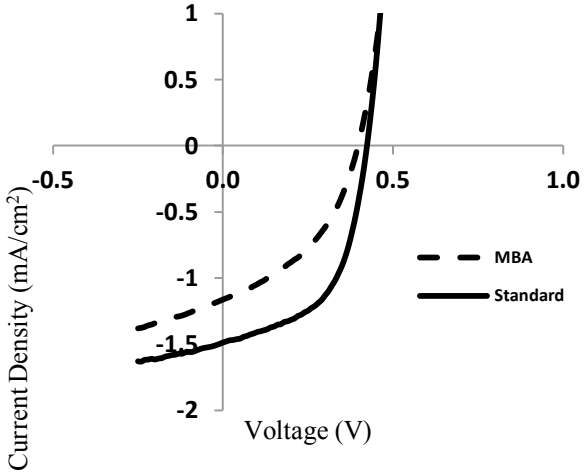

Figure 33: MBA illuminated J-V curve compared to standard.

As seen in the log plots of Figures 30 and 32 there is an apparent decrease in dark current as compared to the standard (ZnO/P3HT) in half of the J-V curve and the other half shows an increase. The logarithmically plotted graphs show an interesting picture because of the fact that there is a crossover point in which the cells go from having a worse, in the sense that there is apparent increase in recombinative effects reflected by the current from the logarithmic dark curve, dark current characteristic to a better one. In a sense it cancels out a part of the constructive dark current decreasing effect, this will be further discussed in section 4.3.3. Under illuminated conditions there is a decrease in short circuit current as compared to the standard and a slight decrease in open circuit voltage. This is observed in Figures 31 and 33. It is interesting to note the similarity in

effect in behavior between these two SAMs as it suggests a negligible effect from the methoxy functional group.

The ABA dark and illuminated curves are shown in Figures 34 and 35.

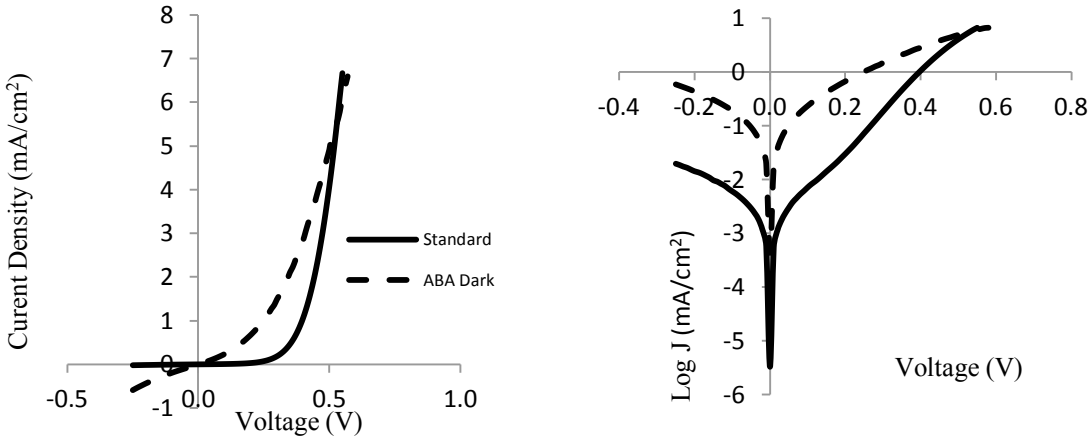

Figure 34: ABA J-V dark curves compared to ZnO standard.

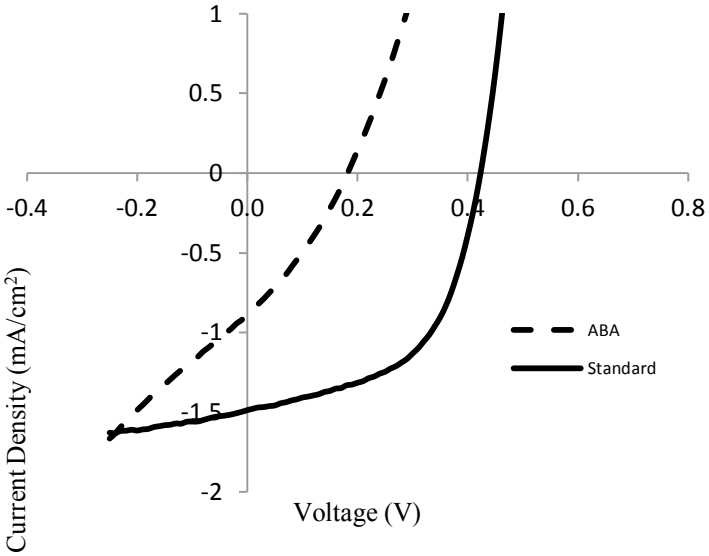

Figure 35: ABA illuminated J-V curve compared to ZnO standard.

It is interesting to note that in the case of ABA there appears to be a very low shunt resistance indicating there is major current leakage in the device. The short circuit current and open circuit voltage were markedly decreased as a result.

Table 3 shows the key parameters of the aforementioned cells.

Table 3: Key Parameters of the benzoic acid derivative cells.

SAM	**V_{OC} (V)**	**J_{SC} ($\frac{mA}{cm^2}$)**	**FF**	**R_{shunt} ($k\Omega*cm^2$)**	**R_{series} ($\Omega*cm^2$)**	**Efficiency (%)**
None	0.42 ± 0.01	1.48 ± 0.1	0.54 ± 0.05	1.5 ± 0.2	21 ± 3	0.34 ± 0.03
BA	0.40 ± 0.01	1.18 ± 0.1	0.43 ± 0.04	1.0 ± 0.1	24 ± 5	0.20 ± 0.02
MBA	0.40 ± 0.01	1.16 ± 0.1	0.42 ± 0.04	1.0 ± 0.1	27 ± 5	0.19 ± 0.01
ABA	0.18 ± 0.01	0.89 ± 0.1	0.31 ± 0.03	0.3 ± 0.1	60 ± 11	0.050 ± 0.005

4.3.3 Phenyl Phosphonic Acid Derivatives

Data are presented for the dark and illuminated curves of PPA and MPPA in Figures 36 through 39.

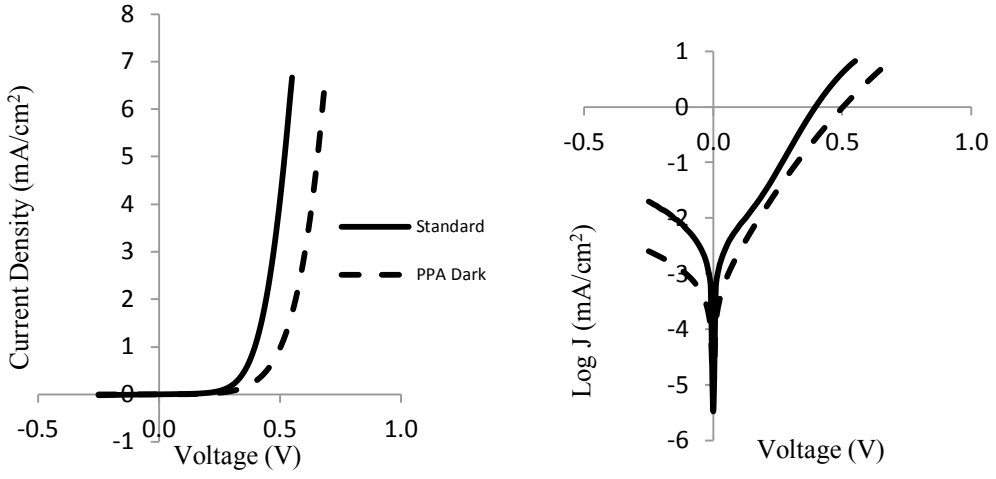

Figure 36: PPA J-V dark curves as compared to ZnO standard.

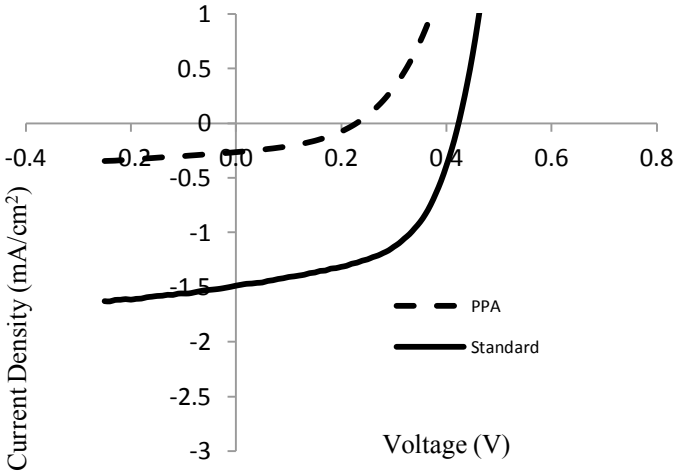

Figure 37: PPA illuminated J-V curve as compared to ZnO standard.

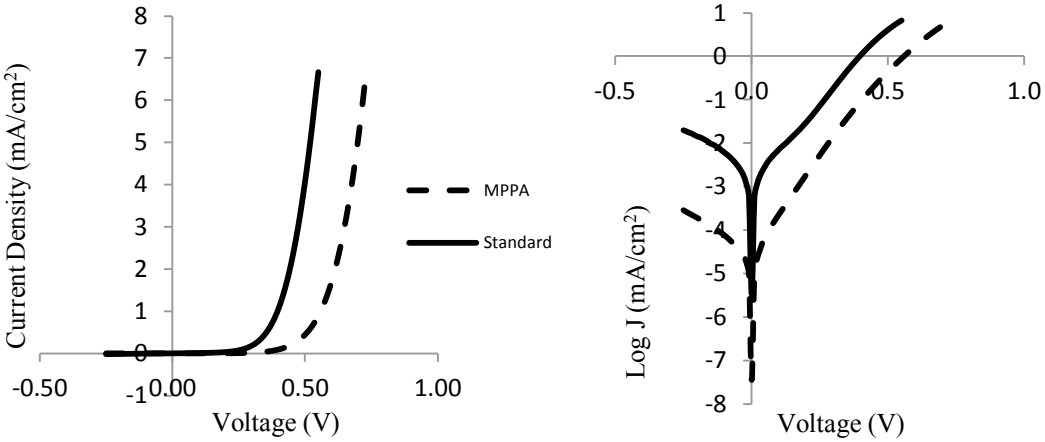

Figure 38: MPPA J-V dark curves as compared to ZnO standard

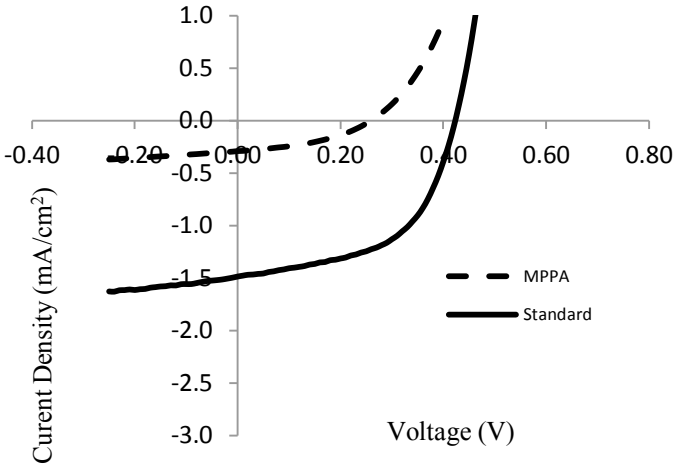

Figure 39: MPPA illuminated as compared to the ZnO standard.

In both cases it is readily apparent that there is a marked decrease in the dark current. However, the illuminated curves indicate that both SAMs have a detrimental effect on short circuit current and open circuit voltage. This will be explained further in section 4.3.3.

Table 4 is a shows the key parameters V_{OC}, J_{SC}, FF, and efficiency of unmodified and phenylphosphonic acid SAM modified cells.

Table 4: Key parameters for the phenylphosphonic acid SAMs.

SAM	**V_{OC} (V)**	**J_{SC} ($\frac{mA}{cm^2}$)**	**FF**	**R_{shunt} (kΩ/ cm^2)**	**R_{series} (kΩ/ cm^2)**	**Efficiency (%)**
None	0.42 ± 0.01	1.48 ± 0.1	0.54 ± 0.05	1.5 ± 0.2	21 ± 3	0.34 ± 0.03
PPA	0.23± 0.01	0.26 ± 0.1	0.40 ± 0.04	3.1 ± 0.5	27 ± 5	0.024 ± 0.002
MPPA	0.26 ± 0.01	0.29 ± 0.1	0.40 ± 0.04	3.1 ± 0.5	30 ± 5	0.031 ± 0.003

4.3.4 Discussion

In Figure 39 a case of an unmodified cell with a surface trap state and a situation in which a cell has a SAM are shown to illustrate the reason for decreased recombination. It is important to note that all SAMs utilized had a benzene base structure. The reason is because of the aromatic nature of the molecule which allows it to conduct electrons using its antibonding π^* orbitals. These antibonding orbitals provide states for electrons coming from the donor to occupy. If not for this feature the molecule would insulate the surface and inhibit electron transport, defeating the purpose of its use in the first place.

It is clear from section 4.3.3 that PPA and MPPA have an effect on decreasing dark current. This is further supported by the shunt resistances which are twice of that observed in a standard cell. This supports the idea that these phosphonic acid derivatives are effective at decreasing recombinative processes.

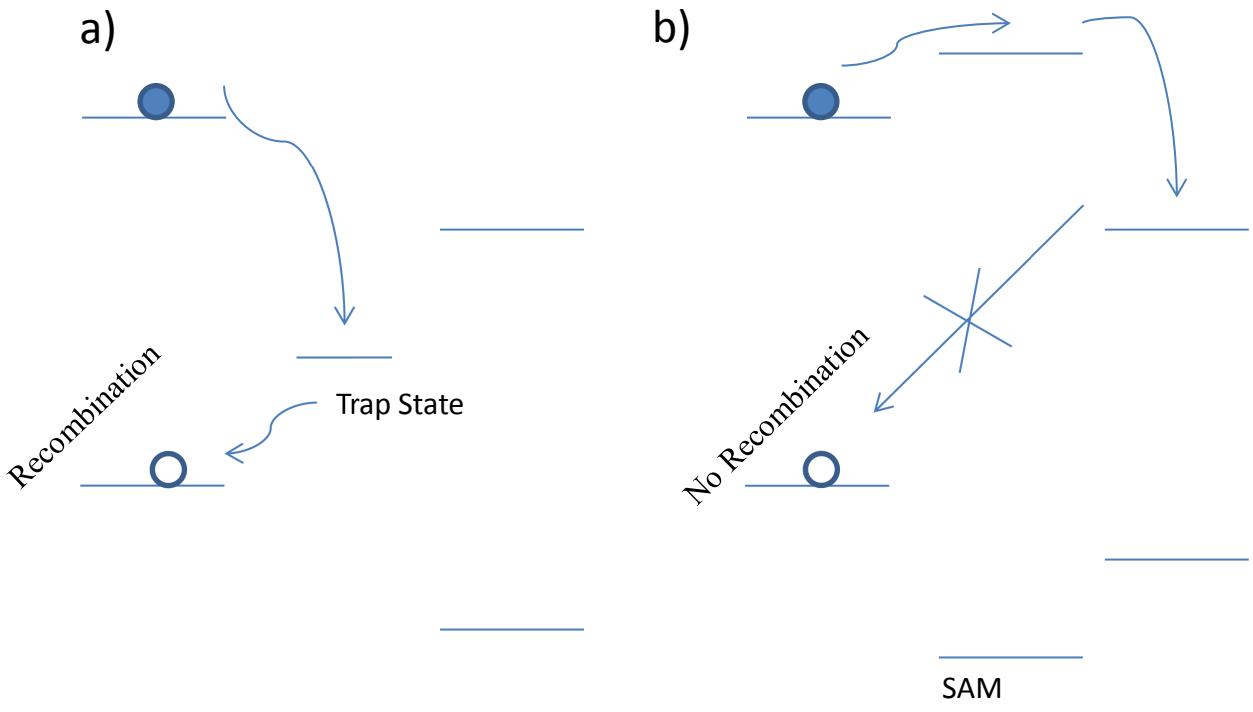

Figure 40: a) Energy levels of Unmodified ZnO with surface trap states providing a recombination site. b) Energy levels of SAM modified ZnO where the SAM is BA, MBA, PPA, or MPPA preventing recombination.

In the case of benzoic acid derivatives, in particular benzoic acid and 4-methoxybenzoic acid, a weak effect on dark current is observed that is partially negated by the fact that in part of the logarithmically plotted J-V curve it increases it and in one part it decreases it as can be seen from Figures 30 and 33. The shunt resistance is smaller than that observed for the standard cell, this indicates that it is leaking current. As for 4-aminobenzoic acid it was shown be ineffectual as a SAM and causes the devices to operate poorly as can be seen from the J-V curves, low shunt resistances, and poor cell parameters as measured for these cells.

The phenylphosphonic acid derivatives, and their benzoic acid counterparts to a lesser extent, hamper device performance. A possible reason is that the SAMs have energy levels that are mismatched in such a way that it makes it harder for the electron to reach the external circuit, but at the same time offer up an energy level well below the acceptor's HOMO which then manifests itself as a decrease in dark current. This is illustrated in Figure 28

A possible reason why the benzoic acid derivatives showed less of an effect on dark current that the phenylphosphonic acids may be because they did not cover the surface of ZnO as effectively. In addition the carboxylic acid group is known to weakly bind to metal oxide surfaces as compared to phosphonic acids.[29,30] It is also a possibility that during the spin coating of the polymer that the benzoic acid SAMs came off or started reorienting themselves, because of their relatively weak adherence, and this could have lead to the unusual J-V curves observed in Figures 30 and 33. Both the higher and lower dark currents in Figures 30 and 33 could be reflecting the lack of orientation in parts of the cell and lack of SAM coverage. To further support this hypothesis the similarly structured phenylphosphonic acids had a significantly more detrimental effect on cell performance, though they should be both binding to the substrate in similar ways. Essentially the devices with BA and MBA were performing better than their phosphonic acid counterparts probably only because there was a lot more uncovered ZnO than SAM covered ZnO.

In the case of ABA there are two possible reasons for the poor performance. The first is that because of the basic nature of the amino group pinholes were being formed in the ZnO film leading to small shorts in the device. It is important to note that measuring the thickness of ZnO after long-term immersion in ABA did not reveal any noticeable changes. It is also possible that the because of the amino group the ZnO film could have too conductive when the SAM was attached. Another possibility is that ABA may have introduced electronic states that were similar in level to trap states shown in Figure 39 a).

CBA lead to cells that malfunctioned and this may have been because of the electron accepting nature of the SAM which effectively would make ZnO an insulator and prohibits electron transfer.

CHAPTER 5 CONCLUSIONS AND RECOMMENDATIONS

Conclusion and recommendations drawn from the course of this work will be made in this section about the use of benzoic and phenylphosphonic acids as SAMs in hybrid ZnO/P3HT solar cells.

5.1 Conclusions

It is apparent from the data collected that PPA and MPPA serve to decrease dark current and therefore recombination in devices. The dark curves shown in Figure 35 for PPA and those shown in Figure 37 for MPPA serve to provide evidence of this point. On the other hand BA and MBA dark curves shown in Figures 29 and 31 respectively show a more ambiguous picture. It is unclear the reasons that in part of the J-V curve there is a decrease in dark current and then in a smaller portion a crossover point where dark current increases. It is possible that with these benzoic acid derivatives, because of the non-uniform coverage of the substrate, there are inhibiting effects on dark current in some regions while in others the molecular orientation might serve to increase the dark current. The non-uniformity of the benzoic acid derivatives on the surface could also have been the reason for the better device performance of these cells under illumination than their phosphonic acid counterparts under illumination, if the assumption is made that a large percentage of the substrate was uncovered ZnO.

It can be concluded from the data collected that phenylphosphonic acids were clearly effective at decreasing dark current in bilayer ZnO/P3HT devices.[11,29] However it should be noted that in both cases the performance of the cells under illumination was impacted negatively and this was likely due to the wide band gap of the materials as shown in Figure 39 b).

As a first attempt at using benzoic acid and phenylphosphonic acid SAMs on the surface of ZnO there are some promising directions that could be taken for ZnO/P3HT cells.

5.2 Recommendations

It is recommended that in the future SAMs be carefully selected by choosing materials with LUMO levels that do not go above the LUMO level of the polymer thus inhibiting electron transport. If a SAM with the property of having a LUMO level between the polymer and ZnO were found it would serve as a preventative against recombinatory mechanisms at the interface and as a result would serve to increase current. It is likely that the kind of SAM needed should be of the phosphonic acid variety as the dark current curves in this dissertation have shown a measure of promise and recent works in the literature seem to be leading in this direction as well.

It would also be ideal to find SAM materials that have a HOMO level higher than the HOMO level of both donor and acceptor to the point where the band gap of the material coincides with the visible spectrum, thereby increasing light absorption in the solar cell. In addition these SAMs could have electron donating functional groups at the end of them in order to tune the work function of the polymer and therefore the open circuit voltage. A suggested route to achieving these goals is suggested.

It would be worthwhile to use a program such as Gaussian to find dipole moments of promising molecules and extrapolate the effects on CPD from the aforementioned CPD versus dipole moment plots. The effect of these SAMs on the donor/acceptor interface could be estimated from such theoretical studies and as a result would provide a good starting point for experimentalists. Once a viable list of SAMs is generated they either need to be fabricated or purchased if available. Once synthesized the SAMs should be thoroughly studied using techniques such as IPES and UPS to determine HOMO and LUMO levels. These SAMs should then be utilized in bilayer ZnO/P3HT devices so their actual effects on solar cell parameters can be ascertained.

It should be noted that in the literature there are long-chain thiophene based phosphonic acids that are being utilized on TiO_2 substrates. These thiophenes also provide a potential avenue for study in the future since they could act as an extra light absorbing layer and

serve to remove trap states from the surface of ZnO thereby inhibit recombinative mechanisms. The issue surrounding thiophene based phosphonic acids use is the difficulty of their synthesis and the very low yields generated.

Another avenue of future research could be to use thiol based SAMs on ZnO. These SAMs have been extensively researched and studied. It may be worth investigating the effects of such SAMs on ZnO since in the literature there has been no indication that they have been used in hybrid solar cell research. Simulation would offer a very important tool in this case as it can provide a basis for what molecular structures should be picked for further study. In addition to being well researched, they can be inexpensive and relatively easy to obtain from commercial suppliers.

Appendix A – Procedure to Make ZnO/P3HT Solar Cell

1) Pattern ITO

- **Set hot plate to 115 C**
- **Spin coat SPR-220 using 3000 RPM 40 s**
- **Anneal for 90 s on the hotplate**
- **Expose to for UV (~360 nm wavelength) 40 s**
- **Anneal 90 s on the hotplate**
- **Put substrate in MF CD-26 developer and swirl for 40 s (should see pattern forming)**
- **Rinse with deionized water**
- **Anneal for 3 minutes on the hotplate**
- **HCl 12 minutes (Rinse with deionized (DI) water thoroughly afterwards). This step removes the ITO from the uncovered regions. It should be noted that immersion time in general is dependent on environmental factors such as temperature and humidity. To suit your particular application takes some trial and error.**
- **Rinse with acetone to remove photoresist**

2) Clean ITO 20 min each in Detergent + Water/Acetone/Isopropanol in a sonicator

3) Spin coat 3 layers ZnO and heat at 300 C on a hotplatefor 10 minutes for each layer. Clean with DI water, isopropanol. Before 1st layer and RIE

4) Remove ZnO edge with a swab dipped in 5% HCl. Dip a swab in deionized water and clean the edges to remove residual HCl.

5) Spin coat P3HT, 20 mg/mL in 1,2 – dichlorobenzene, at 700 rpm 30 s, 1000 rpm for 20 s.

6) Deposit Ag with bell jar thermal evaporation system.

REFERENCES

1. "Solar Energy Perspectives." *IEA*. N.p., n.d. Web. 03 June 2013.

2. Hoppe, Harald, and Niyazi Serdar Sariciftci. "Organic Solar Cells: An Overview." *Journal of Materials Research* 19.7 (2004): 1924-945. Print.

3. Tang, C. W. 2-Layer Organic Photovoltaic Cell. *Appl. Phys. Lett.* **48**, 183-185 (1986).

4. Green, Martin A., Keith Emery, David L. King, Sanekazu Igari, and Wilhelm Warta. "Solar Cell Efficiency Tables(version 39)." *Progress in Photovoltaics: Research and Applications* 12.5 (2011): 365-72. Print.

5. Sekine, Nobuyuki, Cheng-Hsuan Chou, Wei Lek Kwan, and Yang Yang. "ZnO Nano-ridge Structure and Its Application in Inverted Polymer Solar Cell." *Organic Electronics*(2009): n. pag. Print.

6. Nelson, Jenny. *Physics of Solar Cells*. N.p.: World Scientific, 2003. Print.

7. Heggie, Dale A. *Application of a Compositionally Graded Heterojunction for Organic Photovoltaics*. Thesis. Dalhousie University, 2006. N.p.: n.p., n.d. Print.

8. Poly(3-hexylthiophene-2,5-diyl), regioregular Sepiolid P200. (n.d.). *Rieke Metals Main Front Page*. Retrieved May 14, 2013, from http://www.riekemetals.com/index.php?option=com_riekemvc&view=compound&i

9. "An Introduction to the CHA - Concentric Hemispherical Analyser." *An Introduction to the CHA - Concentric Hemispherical Analyser*. N.p., n.d. Web. 24 July 2013.

10. Goh, Chiatzun, Shawn R. Scully, and Michael D. McGehee. "Effects of Molecular Interface Modification in Hybrid Organic-inorganic Photovoltaic Cells." *Journal of Applied Physics* 101.11 (2007): 114503. Print.

11. Ulman, Abraham. "Formation and Structure of Self-Assembled Monolayers." *Chemical Reviews* 96.4 (1996): 1533-554. Print.

12. Halik, Marcus, and Andreas Hirsch. "The Potential of Molecular Self-Assembled Monolayers in Organic Electronic Devices." *Advanced Materials* 23 (2011): 2689-695. Print.

13. Lin, Yun-Yue, Yi-Ying Lee, Liuwen Chang, Jih-Jen Wu, and Chun-Wei Chen. "The Influence of Interface Modifier on the Performance of Nanostructured ZnO/polymer Hybrid Solar Cells." *Applied Physics Letters* 94.6 (2009): 063308. Print.

14. Lee, J. "Electrical and Optical Properties of ZnO Transparent Conducting Films by the Sol–gel Method." *Journal of Crystal Growth* 247.1-2 (2003): 119-25. Print.

15. MEGAPOSIT™SPR-220™ Data Sheet.

16. "Basic Models of Spin Coating." *Professor Robert B. Laughlin, Department of Physics, Stanford University*. N.p., n.d. Web. 21 May 2013.

17. "Operator's Manual: Ultrasonic Cleaners Models 1510, 2510, 3510, 5510, 8510." CPN-214-142. Rev A.

18. "Reactive Ion Etching (RIE) Etching Basics." *RIE Etching*. N.p., n.d. Web. 10 June 2013.

19. Cheung, Nathan. "Reactive Ion Etching." Lecture. *Prof. Yosi Shacham*. Web. 21 May 2013.

20. Trion Phantom II Manual.

21. "Mean Free Path." *, Molecular Collisions*. N.p., n.d. Web. 21 May 2013.

22. KP Technology Manual.

23. Rudy Schlaf. "Tutorial on Kelvin Probe Measurements."

24. Tadmor, Rafael. "Line Energy and the Relation between Advancing, Receding, and Young Contact Angles." *Langmuir* 20.18 (2004): 7659-664. Print.

25. De Gennes, P. G. "Wetting: Statics and Dynamics." *Reviews of Modern Physics* 57.3 (1985): 827-63. Print.

26. Hau, Steven K., Hin-Lap Yip, Orb Acton, Nam Seob Baek, Hong Ma, and Alex K.-Y. Jen. "Interfacial Modification to Improve Inverted Polymer Solar Cells." *Journal of Materials Chemistry* 18.42 (2008): 5113. Print.

27. Taratula, Olena, Elena Galoppini, Dong Wang, Dorothy Chu, Zheng Zhang, Hanhong Chen, Gaurav Saraf, and Yicheng Lu. "Binding Studies of Molecular Linkers to ZnO and MgZnO Nanotip Films." *The Journal of Physical Chemistry B* 110.13 (2006): 6506-515. Print.

28. Krüger, J., U. Bach, and M. Grätzel. "Modification of TiO2 Heterojunctions with Benzoic Acid Derivatives in Hybrid Molecular Solid-State Devices." *Advanced Materials*12.6 (2000): 447-51. Print.

29. Dubey, Manish, Tobias Weidner, Lara J. Gamble, and David G. Castner. "Structure and Order of Phosphonic Acid-Based Self-Assembled Monolayers on Si(100)."*Langmuir* 26.18 (2010): 14747-4754. Print.

30. Liao, Kung-Ching, Hafeez Anwar, Ian G. Hill, Grigory K. Vertelov, and Jeffrey Schwartz. "Comparative Interface Metrics for Metal-Free Monolayer-Based Dye-Sensitized Solar Cells." *ACS Appl. Mater. Interfaces* 4.12 (2012): 6735-746. Print.